Vivo, E., Nicoli, M. y Cuerno, R. (2014). Strong anisotropy in two-dimensional surfaces with generic scale invariance: Nonlinear effects. *Physical Review E*, 89(4), 042407.

DOI: https://doi.org/10.1103/PhysRevE.89.042407

Strong anisotropy in two-dimensional surfaces with generic scale invariance: Nonlinear effects

Edoardo Vivo,[1] Matteo Nicoli,[2] and Rodolfo Cuerno[1]

[1]*Departamento de Matemáticas and Grupo Interdisciplinar de Sistemas Complejos (GISC), Universidad Carlos III de Madrid, Avenida de la Universidad 30, E-28911 Leganés, Spain*

[2]*Center for Interdisciplinary Research on Complex Systems, Department of Physics, Northeastern University, Boston, Massachusetts 02115, USA*

(Received 29 November 2013; published 25 April 2014)

We expand a previous study [Phys. Rev. E **86**, 051611 (2012)] on the conditions for occurrence of strong anisotropy in the scaling properties of two-dimensional surfaces displaying generic scale invariance. In that study, a natural scaling ansatz was proposed for strongly anisotropic systems, which arises naturally when analyzing data from, e.g., thin-film production experiments. The ansatz was tested in Gaussian (linear) models of surface dynamics and in nonlinear models, like the Hwa-Kardar (HK) equation [Phys. Rev. Lett. **62**, 1813 (1989)], which are susceptible of accurate approximations through the former. In contrast, here we analyze nonlinear equations for which such approximations fail. Working within generically scale-invariant situations, and as representative case studies, we formulate and study a generalization of the HK equation for conserved dynamics and reconsider well-known systems, such as the conserved and the nonconserved anisotropic Kardar-Parisi-Zhang equations. Through the combined use of dynamic renormalization group analysis and direct numerical simulations, we conclude that the occurrence of strong anisotropy in two-dimensional surfaces requires dynamics to be conserved. We find that, moreover, strong anisotropy is not generic in parameter space but requires, rather, specific forms of the terms appearing in the equation of motion, whose justification needs detailed information on the dynamical process that is being modeled in each particular case.

DOI: 10.1103/PhysRevE.89.042407 PACS number(s): 68.37.−d, 68.35.Ct, 64.60.Ht, 05.40.−a

I. INTRODUCTION

Scale invariant, two-dimensional surfaces that are anisotropic in space abound in science and technology for systems spanning many orders of magnitude in length scales. Examples range from epitaxial thin films in nanoscience [1], to micro- and macroscopic crack formation in solids [2,3], to geological systems, such as landscape evolution induced by rivers [4,5]. Mathematically, the surfaces that occur in these and many other systems are self-affine fractals [6], whose fractal dimension (or, equivalently, roughness exponent) differs depending on the direction along which it is measured.

Due to the lack of characteristic distances, the scaling behavior just described is a form of anisotropic *critical* behavior [7,8], which moreover often occurs without the need of parameter fine tuning that adjusts the system to a critical point. These are thus examples of so-called generic scale invariance (GSI) [9–11]. Additional well-known instances of space anisotropies ensuing under GSI conditions are driven diffusive systems [12] and self-organized criticality (SOC) [13]. Still another context for this type of behavior, which has remained relatively less studied, is that of surface kinetic roughening [6]. While differing from driven diffusive systems in the fact that dynamics and noise are not necessarily conserved, kinetic roughening systems also differ from SOC systems in the fact that their typical time scales for response are not separated from those characterizing the external driving [10,11].

In this work we pursue a continuum description of GSI systems through stochastic partial differential equations [14]. Within such a framework, our cases of interest will be those conditions that lead to GSI while applying to the most important universality classes in surface kinetic roughening, namely [10,11], systems with nonconserved dynamics, like the celebrated Kardar-Parisi-Zhang (KPZ) equation [15], or systems with conserved dynamics and nonconserved noise, like, e.g., the so-called conserved KPZ (cKPZ) equation [16]. Both equations have been shown to be directly relevant to the growth of two-dimensional interfaces. For instance, the KPZ equation describes the asymptotic behavior of many thin films whose interfacial dynamics is not constrained by conservation laws [6], as, e.g., for silica films grown by chemical vapor deposition [17], while the cKPZ equation plays a cental role in the dynamics of epitaxial surfaces grown by molecular beam epitaxy, in which adatom desorption is typically suppressed, inducing interfacial conservation laws [1].

Remarkably, the anisotropic generalizations of the two previous equations, namely, the so-called anisotropic KPZ (aKPZ) [18] and conserved anisotropic KPZ (caKPZ) equations [19,20], *do not* lead asymptotically to anisotropic behavior (strong anisotropy, SA). Rather, in spite of being nominally anisotropic, they lead to isotropic asymptotics (weak anisotropy, WA) in universality classes that depend on parameter conditions. This fact contrasts strikingly with the unambiguous observation of SA in experiments on surface kinetic roughening for two-dimensional interfaces; see [21] and references therein. To cite a few, anisotropic behavior occurs for growth by molecular beam epitaxy, both under morphologically unstable conditions, as for growth on Si(001) [22–24], or for morphologically stable ones, as for growth of GaAs films [25,26]. Also, erosion, rather than growth, of thin films by ion-beam sputtering (IBS) induces space anisotropies related to the different roles played by the direction on the target that lies along the projection of the ion beam and the direction perpendicular to it, leading to strong anisotropy regardless of the morphological stability conditions of the experiment [27,28]. Macroscopically, fracture of solids

provides still another instance for the occurrence of space anisotropies, in this case between the crack propagation and crack front directions [2,3], and concomitant SA properties.

Ansätze for anisotropic kinetic roughening

The previous facts underscore the lack of a sufficient understanding of strongly anisotropy kinetic roughening for the case of two-dimensional interfaces, with particular experimental relevance. Actually, the interface equations that can potentially describe a range of anisotropic systems still remain to be identified, as is the case, e.g., for IBS systems [29]. This motivated us to perform a systematic study of the phenomenon, with the aim to identify general conditions on the occurrence of isotropic vs anisotropic behavior. Our program started with the formulation of a scaling ansatz for strong anisotropy [30], as encoded in the asymptotic behavior of the surface structure factor, that could be readily applied to analyze experimental data on, say, surface dynamics of thin films [21]. Specifically, suppose the scalar field $h(\mathbf{r})$ describes the height of a surface above point $\mathbf{r} = (x,y)$ on a reference plane. A convenient characterization of its fluctuations can be performed through the power spectral density (PSD) or height structure factor [6],

$$S(\mathbf{k}) = \langle |h_{\mathbf{k}}|^2 \rangle, \tag{1}$$

where $\mathbf{k} = (k_x,k_y)$ is the wave vector, $h_{\mathbf{k}}$ is the space Fourier transform of $h(\mathbf{r})$, and brackets denote averages over the noise distribution. For a system displaying SA, we postulate [30] that the stationary PSD scales with wave-vector components k_x and k_y as

$$S(k_x,k_y) \sim \frac{1}{k_x^{2\tilde{\alpha}_x} + \nu k_y^{2\tilde{\alpha}_y}}, \tag{2}$$

where we refer to $\tilde{\alpha}_x$ and $\tilde{\alpha}_y$ as roughness exponents in momentum space and ν is a mere constant. It is convenient to also make contact with observables in real space, such as the two-dimensional (2D) height-difference correlation function

$$G(r) = \langle [h(\mathbf{r}+\mathbf{r}_0) - h(\mathbf{r}_0)]^2 \rangle, \tag{3}$$

where $\mathbf{r}_0 = (x_0,y_0)$ is an arbitrary position on the substrate plane and $r = |\mathbf{r}|$. Indeed, a natural, equivalent definition of SA is that the value of the roughness exponent changes with the direction along the latter. Namely, by defining 1D versions of the height-difference correlation function along the two substrate directions,

$$G_x(x) = \langle [h(x_0+x,y_0) - h(x_0,y_0)]^2 \rangle, \tag{4}$$

$$G_y(y) = \langle [h(x_0,y_0+y) - h(x_0,y_0)]^2 \rangle, \tag{5}$$

and under kinetic roughening conditions, scaling behavior ensues [6], $G_x(x) \sim x^{2\alpha_x}$ and $G_y(y) \sim y^{2\alpha_y}$, where $\alpha_{x,y}$ are two potentially different roughness exponents. The system is said to display SA if indeed $\alpha_x \neq \alpha_y$, whereas WA occurs when the steady state of the system is actually *isotropic*, so that $\alpha_x = \alpha_y = \alpha$, with $G(r) \sim r^{2\alpha}$ in such a case. In Ref. [30] we proved that, indeed, Eq. (2) is equivalent to SA for the correlation functions (4) and (5), provided exponents are related as

$$2\alpha_x = 2\tilde{\alpha}_x - \zeta - 1, \tag{6}$$

$$2\alpha_y = 2\tilde{\alpha}_y - 1/\zeta - 1, \tag{7}$$

where we have introduced the anisotropy exponent

$$\zeta = \frac{\tilde{\alpha}_x}{\tilde{\alpha}_y} = \frac{\alpha_x}{\alpha_y}, \tag{8}$$

the second equality being a consequence of Eqs. (6) and (7). Thus, SA is simply stated as $\zeta \neq 1$. Conversely, WA implies $\zeta = 1$, so that $\alpha_x = \alpha_y = \alpha$ and Eq. (2) is asymptotically equivalent to the isotropic behavior of the 2D PSD function [6] $S(\mathbf{k}) \sim k^{-(2\alpha+2)}$, with $k = |\mathbf{k}|$.

In turn, as an alternative to the 1D correlation functions (4) and (5), one may consider the power spectral densities $S_x(k_x)$ and $S_y(k_y)$ of 1D cuts of the 2D interface along the x and y directions. In many experimental or numerically simulated systems, this is a way to improve over the signal-to-noise ratio of the 2D PSD. Thus, for instance, considering a fixed value $y = y_0$, one defines

$$S_x(k_x) = \langle h_{k_x}^{(y_0)} h_{-k_x}^{(y_0)} \rangle, \tag{9}$$

where $h_{k_x}^{(y_0)}$ is the Fourier transform of the corresponding 1D profile $h(x,y_0)$. Analogously, one can define $S_y(k_y)$ for a cut along the y direction at a fixed $x = x_0$ value. As a consequence of Eq. (2), these functions scale as [30,31]

$$S_x(k_x) \sim k_x^{-(2\tilde{\alpha}_x - \zeta)} = k_x^{-(2\alpha_x+1)}, \tag{10}$$

$$S_y(k_y) \sim k_y^{-(2\tilde{\alpha}_y - 1/\zeta)} = k_y^{-(2\alpha_y+1)}, \tag{11}$$

which provide the natural generalization to the SA case of the scaling behavior of the PSD of 1D cuts of the surface in the isotropic case, in which $\alpha_x = \alpha_y = \alpha$ and $S_{x,y} \sim k_{x,y}^{-(2\alpha+1)}$ [6,32].

With respect to the time evolution, the isotropic behavior is encoded in the standard Family-Vicsek (FV) ansatz for kinetic roughening of surfaces, which is typically formulated in terms of the surface roughness $W^2(t) = \langle (h-\bar{h})^2 \rangle = \int S(\mathbf{k})\, d\mathbf{k}$. Thus [6], $W \sim t^{\beta}$ for $t \ll L^z$, while $W \sim L^{\alpha}$ for $t \gg L^z$, where z is the so-called dynamic exponent, $t^{1/z}$ is proportional to the length scale below which nontrivial correlations have built up among height values at different substrate positions, L is the lateral system size, and $\beta = \alpha/z$ is usually termed the growth exponent. As shown in [30], for strongly anisotropic systems, the ansatz (2) implies that the behavior of the roughness of 1D line profiles is $W_{x,y} \sim t^{\beta}$ for $t \ll L^{z_{x,y}}$, while $W_{x,y} \sim L^{\alpha_{x,y}}$ for $t \gg L^{z_{x,y}}$. Namely, there are two dynamic exponents $z_{x,y}$, which are related as $z_y = z_x/\zeta$, and a single growth exponent, since then $\beta_x = \alpha_x/z_x = \beta_y = \alpha_y/z_y = \beta$. Indeed, for $\zeta = 1$ one has that $\alpha_x = \alpha_y = \alpha$ and $z_x = z_y = z$, and WA ensues. This SA dynamic behavior has been confirmed in the experiments of Ref. [21]. Overall, for a strongly anisotropic system there are then three independent critical exponents, e.g., α_x, z_x, and ζ.

Note that, although anisotropic kinetic roughening was previously encoded into a scaling ansatz [33] originating in the study of critical dynamics of equilibrium statistical-mechanical systems [34], such a theoretically powerful formulation is not particularly natural for the characterization of actual 2D surfaces. In Refs. [21,30] we have clarified the relation between Eq. (2) and the behavior of standard observables employed in the experimental characterization of anisotropic thin films through, e.g., 1D correlations like $G_{x,y}$ or power spectral densities of 1D profiles, $S_{x,y}$. We have

moreover shown how all these results can be employed in a consistent characterization of SA for actual experimental data on ion beam-sputtered silicon surfaces [21].

Frequently, e.g., in the molecular beam epitaxy or IBS systems mentioned above, physical properties and geometric constraints dictate the appropriate choices for the x and y directions. Still, as shown in [30], under conditions for SA, any choice of two orthogonal directions will lead to the same set of two different exponents $\tilde{\alpha}_{x,y}$, which guarantees the generality of ansatz (2). In the case of, e.g., fracture, alternative choices for anisotropic scaling ansätze are also available, in which, e.g., either an auxiliary dynamics is postulated [3,35] or expansions of observables over appropriate functional bases are performed that exploit the fact that isotropic materials often have anisotropic fracture surfaces only because of the breaking of isotropy by the initial conditions [36,37].

From the theoretical point of view, ansatz (2) was motivated by the behavior of exact solutions to linear interface equations displaying SA and was further validated in Ref. [30] against a nonlinear system for which SA is also well known to occur, namely, the Hwa-Kardar (HK) equation [38,39]. This equation was originally put forward to describe the evolution of the surface height for a running sand pile, a particular instance of a supercritical SOC system. The equation has conserved dynamics, reflecting the conservation in the number of sand grains by the relaxation dynamics, and nonconserved noise, as a reflection of the nonconserved driving field associated with sand-grain addition. Thus, it features GSI, characterized by anisotropic scaling exponents which are believed to be exact [38,39]. As it turns out, one can write an exactly solvable, linear equation with the same exponents [30], which makes it possible to elucidate superficial differences between the SA scaling of the HK equation and ansatz (2) as being due to finite size effects [30].

In this work, we pursue further the study of SA through continuum interface equations by trying to identify conditions that such models have to fulfill in order to display this type of scaling. This characterization might prove useful when invoking universality principles [40,41] in order to put forward a continuum equation for a system featuring SA. To this end, we focus on a number of representative equations, all of which display GSI and which remained outside the analysis in [30], due to the unavailability of accurate approximations through linear equations for most of the cases. Thus, we employ techniques that, in principle, can tackle strongly nonlinear systems, such as the dynamic renormalization group and direct numerical simulations.

In the presence of conserved dynamics, we recall results for the paradigmatic caKPZ equation (which, as mentioned, displays WA) and generalize this equation into a related system which presents SA. Likewise, given that the HK equation has a special form that does not admit an isotropic limit, we provide a natural generalization of it which does. However, this equation turns out to again display WA. Interestingly, while the caKPZ equation is invariant under a global shift of the height values $h \to h + \text{const.}$, the (generalized) HK equation is not. Nevertheless, the overall behavior with respect to SA seems common. Thus, as a partial conclusion, we note that SA can appear for conserved dynamics, but it requires a form of the interface equation that is not generic in parameter space. Actually, as argued with some generality in [42], anisotropies do seem to play a more relevant role in the conserved dynamics case than for nonconserved dynamics. We confirm this in our present context by revisiting the paradigmatic representative of nonconserved dynamics, namely, the aKPZ equation. Even analyzing some particular limits that had remained unexplored thus far, we confirm the general conclusion on the occurrence of WA throughout parameter space for this model.

The paper is organized as follows. Section II contains a brief reminder on the basic steps of the analytical technique we employ in order to study the SA properties of the equations just mentioned, namely, the dynamic renormalization group (DRG). This allows us to establish our notation and some assumptions which are common to all cases discussed. Section III is devoted to equations with conserved dynamics, while the case of nonconserved dynamics is explored in Sec. IV. We extract conclusions on modeling of strongly anisotropic systems in the final section, Sec. V. Finally, we provide two appendixes with details on our DRG calculations for the generalized HK equation and for the aKPZ equation. While the former is a new model, the latter has been long studied in the literature [18], although in a short account. We hope these details can be found to be useful by the interested reader.

II. DYNAMIC RENORMALIZATION GROUP

In this section we review briefly the main steps taken by the analytical technique which is extensively used in this work. As mentioned earlier, we address nonlinear equations, trying to extract the scaling exponents α_x, ζ, and z_x which are predicted in each case. While for linear stochastic equations such as those considered in [30], values for the latter can be readily extracted from a simple rescaling of coordinates and fields [6]; in general, this is not the case in the presence of nonlinearities. For these, it is a nontrivial balance between the linear and the nonlinear operators occurring in the equation which controls its asymptotic behavior. The DRG is a standard perturbative approach to elucidate the interplay among these terms. Originally, the method was developed in the contexts of fluctuating hydrodynamics [43] and dynamic critical phenomena [44]. More recently, it has been successfully applied to understand, e.g., the multiscale nature of fluctuating interfaces [45], kinetic roughening in surfaces controlled by unstable nonlocal interactions [46,47], or the interplay between noise and morphological instabilities in anisotropic pattern-forming systems [48,49], to cite a few examples.

Here we sketch the main steps involved in our DRG analysis. These are later applied in a number of cases, computational details being provided in the appendixes. For the systems that are addressed, both linear and nonlinear terms share similar structures when written in Fourier-space coordinates $\mathbf{k}$. Specifically, the nonlinear evolution equations to be studied in the next sections can be written as

$$\partial_t h_{\mathbf{k}}(t) = \sigma_{\mathbf{k}} h_{\mathbf{k}}(t) + \lambda_x \mathcal{N}_x[h, \nabla h]_{\mathbf{k}} + \lambda_y \mathcal{N}_y[h, \nabla h]_{\mathbf{k}} + \eta_{\mathbf{k}}(t), \tag{12}$$

where, in general, $\mathbf{k}$ is wave vector in d-dimensional Fourier space, although we consider $d = 2$ in our specific cases. The fluctuating term η is taken as a Gaussian white noise with zero

mean and variance equal to $2D$. For the sake of generality, at this moment we leave the linear dispersion relation $\sigma_{\mathbf{k}}$ unspecified. With respect to the nonlinear operators $\mathcal{N}_{x,y}$, they also remain generic, except for the fact that they are *bilinear* products of the height field h and its space derivatives—such as, e.g., $(\partial_x h)^2, h\partial_x h$, etc.—with $\lambda_{x,y}$ being representative nonlinear coupling constants. Although most of the equations we study include two different nonlinear couplings, for the sake of simplicity in illustrating the procedure, in the remainder of this section we consider a single one. The first step of the DRG procedure consists of time-Fourier transforming Eq. (12),

$$[-\sigma_{\mathbf{k}} - i\omega]h_{\mathbf{k},\omega} = \eta_{\mathbf{k},\omega} + \lambda \int_{|\mathbf{q}|\leqslant\Lambda} \frac{d\mathbf{q}}{(2\pi)^d} \int_{-\infty}^{+\infty} \frac{d\Omega}{2\pi} \times f_1(\mathbf{q},\mathbf{k})\, h_{\mathbf{q},\Omega} h_{\mathbf{k}-\mathbf{q},\omega-\Omega}, \quad (13)$$

where ω is time frequency and $\Lambda = \pi/\Delta x$ is the wave number cutoff in the system, Δx being the lattice spacing in real space. The specific form of the function $f_1(\mathbf{q},\mathbf{k})$ depends on that of the nonlinear term $\mathcal{N}$ in the equation. In Fourier space, the noise term still has zero mean $\langle \eta_{\mathbf{k},\omega}\rangle = 0$ and is δ correlated, but its variance becomes rescaled as

$$\langle \eta_{\mathbf{k},\omega}\eta_{\mathbf{k}',\omega'}\rangle = 2D(2\pi)^{d+1}\,\delta_{\mathbf{k}+\mathbf{k}'}\,\delta_{\omega+\omega'}. \quad (14)$$

Following the standard Forster-Nelson-Stephen procedure [43], we define a square shell, parametrized by a real number $b = e^{\delta l} > 1$, such that the height and the noise fields are split into two types of components, slow modes $h^<_{\mathbf{k},\omega}$, $\eta^<_{\mathbf{k},\omega}$ for $k_{x,y} \in (0, \Lambda/b)$, and fast modes $h^>_{\mathbf{k},\omega}$, $\eta^>_{\mathbf{k},\omega}$ for $k_{x,y} \in [\Lambda/b, \Lambda]$. Frequently, for isotropic systems the square shell is approximated by a circular one, with internal radius Λ/b and external radius given by Λ. However, when dealing with anisotropic equations, the coarse-graining procedure has to be performed separately for k_x and k_y, and the resulting shell will be rectangular, rather than square [20,48]. We have taken this fact into account in the DRG calculations that are shown below.

For infinitesimal δl, a small amount of fast modes is eliminated by solving perturbatively the equation for the modes $h^>_{\mathbf{k},\omega}$, substituting this solution into the equation for the slow modes and assuming statistical independence between high- and low-frequency components. Formally, the small parameter in the perturbative expansion is the strength of the nonlinear term, λ. This procedure leads to an effective equation in which the fast modes are thus integrated out,

$$[-\sigma_{\mathbf{k}} - \Sigma(\mathbf{k},0) - i\omega]h^<_{\mathbf{k},\omega} = \eta^<_{\mathbf{k},\omega} + \lambda \int_< \frac{d\mathbf{q}}{(2\pi)^d} \int \frac{d\Omega}{2\pi}\, f_1(\mathbf{q},\mathbf{k}) h^<_{\mathbf{q},\Omega} h^<_{\mathbf{k}-\mathbf{q},\omega-\Omega} + \mathrm{O}(\lambda^3). \quad (15)$$

The effect of this coarse-graining procedure (i.e., the elimination of the fast modes) is obtained by solving the integral

$$\Sigma(\mathbf{k},\omega) = \lambda^2 D \int_> \frac{d\mathbf{q}}{(2\pi)^d} \int \frac{d\Omega}{2\pi}\, f_2(\mathbf{q},\mathbf{k}) G_0(\mathbf{q},\Omega) \times G_0(-\mathbf{q},-\Omega) G_0(\mathbf{k}-\mathbf{q},\omega-\Omega), \quad (16)$$

where the function $f_2(\mathbf{q},\mathbf{k})$ depends on the exact form of the nonlinearity. To lighten the notation, in the last two expressions we have omitted the integration limits in the frequency domain, and we have denoted the integrals over the fast (slow) modes as $\int_>$ ($\int_<$). In Eq. (16) we have introduced the bare propagator $G_0(\mathbf{k},\omega) = (-\sigma_{\mathbf{k}} - i\omega)^{-1}$, whereas on the left-hand side of Eq. (15) the coarse-grained propagator appears, namely,

$$G^<_0(\mathbf{k},\omega) \equiv [-\sigma_{\mathbf{k}} - \Sigma(\mathbf{k},0) - i\omega]^{-1}. \quad (17)$$

From this last expression it is obvious that only the parameters appearing in the dispersion relation are affected by the coarse graining of the propagator.

The second parameter of the system that is renormalized is the variance of the noise term. From the equation

$$\langle h^<_{\mathbf{k},\omega} h^<_{-\mathbf{k},-\omega}\rangle = 2D^< G^<_0(\mathbf{k},\omega) G^<_0(-\mathbf{k},-\omega), \quad (18)$$

we can easily derive

$$\langle \eta^<_{\mathbf{k},\omega}\eta^<_{-\mathbf{k},-\omega}\rangle = 2[D^< + \Phi(\mathbf{k},0)](2\pi)^{d+1}\,\delta_{\mathbf{k}+\mathbf{k}'}\,\delta_{\omega+\omega'} + \mathrm{O}(\lambda^3), \quad (19)$$

where the coarse-grained noise variance is given by

$$\Phi(\mathbf{k},\omega) = \lambda^2 D^2 \int_> \frac{d\mathbf{q}}{(2\pi)^d} \int \frac{d\Omega}{2\pi}\, f_3(\mathbf{q},\mathbf{k})\, |G_0(\mathbf{q},\Omega)|^2 \times |G_0(\mathbf{k}-\mathbf{q},\omega-\Omega)|^2. \quad (20)$$

As before, $f_3(\mathbf{q},\mathbf{k})$ depends on the details of the nonlinearity for each case considered.

The last step of the coarse-graining procedure has to deal with the corrections to the nonlinear coupling λ, which can be read off from the perturbative expansion that makes it possible to rewrite Eq. (15) with the same structure as Eq. (12), but with modified parameters. However, as we have already demonstrated in [47], for a large class of nonlinearities this parameter does not renormalize. The systems we consider here have exactly this kind of behavior.

Finally, after coarse-graining of propagator, noise variance, and nonlinearities, the final step in the DRG method is a rescaling that restores the value of the ensuing wave vector cutoff, Λ/b, to its bare value Λ. Within the small δl approximation, this moreover makes it possible to write parameter renormalization in a differential form, taking l as the independent variable. Note that, for anisotropic equations, the rescaling of the x and y coordinates has to be done in an anisotropic way as well, as done, e.g., in Eq. (25); see below.

III. CONSERVED DYNAMICS

We start by considering systems for which dynamics are conserved. Recall that, in contrast with nonconserved dynamics, in such a case GSI ensues if noise is nonconserved [10,11], irrespective of whether the deterministic part of the dynamical equation is or not invariant under arbitrary global changes in the value of the height $h(\mathbf{r},t) \to h(\mathbf{r},t) + \text{const}$. We thus consider two representative examples, one in which such *shift invariance* occurs and a different one in which it does not.

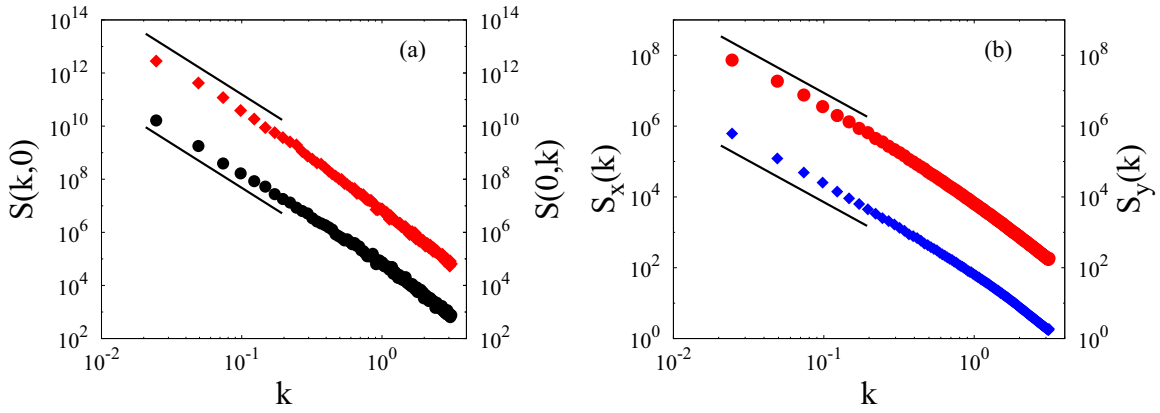

FIG. 1. (Color online) Numerical integrations of Eq. (23) for parameters $\nu_x = \nu_y = 1$, $D = 1$, $\lambda_x = -3$, $\lambda_y = -1$, $L = 256$, $\Delta x = 1$, and $\Delta t = 0.05$. (a) One-dimensional projections $S(k,0)$ (black circles, left axis) and $S(0,k)$ (red diamonds, right axis) of the 2D PSD, averaged over 100 different noise realizations. The solid black lines are guides for the eye with slope $-10/3$. (b) PSD of 1D cuts $S_x(k)$ (blue diamonds, left axis) and $S_y(k)$ (red circles, right axis). The solid black lines are guides for the eye with slope $-7/3$. For visualization purposes, the values of $S(0,k)$ and $S_y(k)$ have been artificially offset vertically. All units are arbitrary.

A. Systems with shift invariance: Conserved anisotropic KPZ equation

A conceptually important example of an anisotropic conserved equation with nonconserved noise, which is invariant under arbitrary shifts of the height, is the caKPZ equation. This model has been formulated and studied [19,20] in the context of nonequilibium growth of epitaxial thin films, specifically for surfaces which are vicinal to a high symmetry surface [1]. Specifically, the caKPZ equation reads

$$\partial_t h = -\nabla^2\left[\nu_x\partial_x^2 h + \nu_y\partial_y^2 h + \frac{\lambda_x}{2}(\partial_x h)^2 + \frac{\lambda_y}{2}(\partial_y h)^2\right] + \eta, \tag{21}$$

where a linear first-order derivative term has been omitted, which does not affect our discussion and conclusions [19]. In Eq. (21), $\nu_{x,y} > 0$ and $\lambda_{x,y}$ are constant parameters. Note that dynamics are explicitly conserved while noise is not, and the equation only depends on h through its space or time derivatives, so that the equation does not single out any preferred height value. For generic parameter values, the DRG analysis performed in [19,20] leads to the conclusion that the system shows WA (i.e., $\zeta = 1$), displaying the scaling exponents of the isotropic conserved KPZ equation, which reads [16]

$$\partial_t h = -\nabla^2\left[\nu\nabla^2 h + \frac{\lambda}{2}(\boldsymbol{\nabla} h)^2\right] + \eta. \tag{22}$$

Specifically, for $d = 2$ the scaling exponents of the caKPZ equation are thus predicted to be approximately given through a one-loop DRG analysis [16] (small corrections occur within a two-loop calculation [50]) by $\alpha \simeq 2/3$ and $z \simeq 10/3$. In particular, the change of universality class that occurs in the nonconserved anisotropic KPZ equation when changing the relative signs of the nonlinearities from nonlinear behavior for $\lambda_x\lambda_y > 0$ to linear behavior for $\lambda_x\lambda_y < 0$ does not occur for the caKPZ equation [19,20].

In order to further discuss the scaling properties of the caKPZ equation, we first consider a similar model that shares with it the behavior just described. Thus, consider the equation

$$\partial_t h = -\nu_x\partial_x^4 h - \nu_y\partial_y^4 h - \frac{\lambda_x}{2}\partial_x^2(\partial_x h)^2 - \frac{\lambda_y}{2}\partial_y^2(\partial_y h)^2 + \eta. \tag{23}$$

The main difference between Eqs. (21) and (23) is that each term in the latter, e.g., $-\frac{\lambda_x}{2}\partial_x^2(\partial_x h)^2$, is affected by an overall second-order derivative operator with a reduced symmetry as compared to its counterpart in the former, e.g., $-\frac{\lambda_x}{2}\nabla^2(\partial_x h)^2$. Nevertheless, the scaling behavior is not modified, as we have verified by numerical simulations. Specifically, we have integrated Eq. (23) by means of a pseudospectral integration algorithm as described in [51] and references therein. The results of the simulations are presented in Figs. 1 and 2.

Thus, the left and right panels of Fig. 1 show, respectively, cuts of the 2D PSD function $S(\mathbf{k})$ along the coordinate axes in $\mathbf{k}$ space and 1D PSD functions for cuts of the surface along the x and y directions, $S_{x,y}(k_{x,y})$, for a condition of Eq. (23) in which $\lambda_x\lambda_y > 0$. Agreement with asymptotic scaling behavior as in Eqs. (2), (6), (7), (10), and (11) for a WA case is very good, using the expected exponents for the isotropic cKPZ equation, $\alpha_x = \alpha_y \simeq 2/3$. Similar agreement is obtained in Fig. 2 for a condition of Eq. (23) in which $\lambda_x\lambda_y < 0$. Therefore, the scaling exponents correspond to those of the isotropic cKPZ equation, irrespective of the relative signs of the nonlinearities, so we can safely say that Eq. (23) is in the same universality class as the caKPZ equation, Eq. (21).

Having established the previous result, the only possibility for Eq. (23), and equivalently for the caKPZ equation, to display strongly anisotropic behavior is that one nonlinearity, say λ_y, is suppressed, but not the other. Hence, we consider equation

$$\partial_t h = -\nu_x\partial_x^4 h - \nu_y\partial_y^4 h - \frac{\lambda_x}{2}\partial_x^2(\partial_x h)^2 + \eta. \tag{24}$$

In a specific physical situation, this implies a nongeneric parameter condition, e.g., that the corresponding nonlinear contribution to the surface-diffusion current vanishes [6] due to a special parameter choice. This case seems not to have been

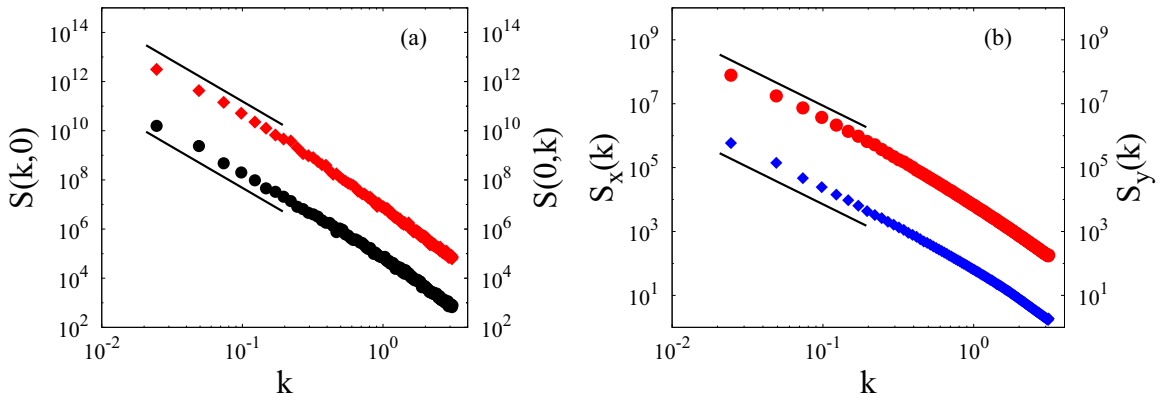

FIG. 2. (Color online) Numerical integrations of Eq. (23) for parameters $\nu_x = \nu_y = 1$, $D = 1$, $\lambda_x = -3$, $\lambda_y = 1$, $L = 256$, $\Delta x = 1$, and $\Delta t = 0.05$. (a) One-dimensional projections $S(k,0)$ (black circles, left axis) and $S(0,k)$ (red diamonds, right axis) of the 2D PSD, averaged over 100 different noise realizations. The solid black lines are guides for the eye with slope $-10/3$. (b) PSD of 1D cuts $S_x(k)$ (blue diamonds, left axis) and $S_y(k)$ (red circles, right axis). The numerical integrations were performed for the same parameters as in the left panel. The solid black lines are guides for the eye with slope $-7/3$. For visualization purposes, the values of $S(0,k)$ and $S_y(k)$ have been artificially offset vertically. All units are arbitrary.

considered in [19]. Actually, we can benefit from the DRG analysis performed by Kallabis in order to derive expectations for the critical exponents of Eq. (24): After the coarse-graining step is performed (full details are available in [20]) as described in Sec. II, we perform an anisotropic rescaling that restores the original wave-vector cutoff, namely,

$$x \to bx, \quad y \to b^{\zeta} y, \quad t \to b^{z_x} t, \quad h \to b^{\alpha_x} h. \tag{25}$$

Using $b = e^{\delta l}$ and taking into account the net modification of the equation parameters after both the coarse-graining and the rescaling transformations, the DRG parameter flow for ν_y, λ_x, and D reads particularly simple, namely,

$$\frac{d\nu_y}{dl} = \nu_y(z_x - 4\zeta), \tag{26}$$

$$\frac{d\lambda_x}{dl} = \lambda_x(\alpha_x + z_x - 4), \tag{27}$$

$$\frac{dD}{dl} = D(z_x - 2\alpha_x - \zeta - 1), \tag{28}$$

which actually coincides with the result of a mere parameter rescaling [6]. The reasons behind such a simplicity are as follows. (i) Given that in Eq. (24) $\lambda_y = 0$ to begin with, parameter renormalization can be only due to the remaining nonlinearity λ_x, which does not contribute to k_y^2 order; hence, ν_y does not renormalize. (ii) At one-loop order there is a vertex cancellation [47] by which λ_x does not renormalize either. (iii) As standard for conserved equations with nonconserved noise, since the lowest-order nonlinear modification of the noise propagator is $O(k_x^2)$, the variance D is not affected and it does not renormalize either. Finally, the fixed points of the RG flow control the scaling behavior. Thus, setting to zero the right-hand sides of Eqs. (26)–(28) we obtain

$$z_x = 4\zeta, \tag{29}$$

$$\alpha_x + z_x = 4, \tag{30}$$

$$z_x = 2\alpha_x + \zeta + 1. \tag{31}$$

These are three equations for three unknowns, whose solution does correspond to SA behavior, namely,

$$\alpha_x = 8/11, \quad z_x = 36/11, \quad \zeta = 9/11. \tag{32}$$

We have performed numerical simulations of Eq. (24) in order to verify Eq. (32). The results, presented in Fig. 3, are in good agreement with these SA values of the scaling exponents.

In spite of being strongly anisotropic, the ζ value obtained for Eq. (24) is very close to one, so that effectively scaling behavior is not far from a proper weakly anisotropic case. For practical applications, Eq. (24), and thus the caKPZ equation with $\lambda_y = 0$, is not the most clear-cut example of SA. However, Eqs. (29)–(31) give us a way to construct an equation similar to (24), but with a tunable anisotropy exponent ζ. In wave-vector space, such an equation can be written as

$$\partial_t h = -(\nu_x |k_x|^{2n+2} + \nu_y |k_y|^{2m}) h_{\mathbf{k}} - \frac{\lambda_x}{2} |k_x|^{2n} \mathcal{F}[(\partial_x h)^2] + \eta_{\mathbf{k}}, \tag{33}$$

where $\mathcal{F}[\cdot]$ denotes space Fourier transform, and n and m are *real* numbers. Notice that Eq. (24) corresponds simply to the particular choice $n = 1$ and $m = 2$. In exactly the same form as Eqs. (29), it is not difficult to derive scaling relations for Eq. (33),

$$\alpha_x + z_x = 2(n+1), \tag{34}$$

$$z_x = 2m\zeta, \tag{35}$$

$$z_x = 2\alpha_x + 1 + \zeta, \tag{36}$$

whose solution provides the following values of the exponents as functions of n and m:

$$\alpha_x = \frac{4nm + 2m - 2n - 2}{6m - 1}, \tag{37}$$

$$z_x = 2m\frac{4n+5}{6m-1}, \tag{38}$$

$$\zeta = \frac{4n+5}{6m-1}. \tag{39}$$

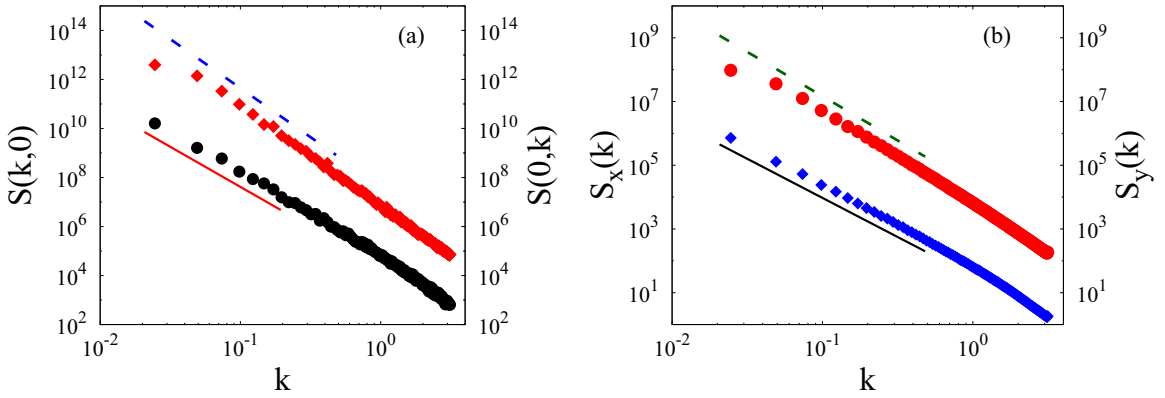

FIG. 3. (Color online) Numerical integrations of Eq. (24) for parameters $\nu_x = \nu_y = 1$, $D = 1$, $\lambda_x = 3$, $L = 256$, $\Delta x = 1$, and $\Delta t = 0.05$. (a) One-dimensional projections $S(k,0)$ (black circles, left axis) and $S(0,k)$ (red diamonds, right axis) of the 2D PSD, averaged over 100 different noise realizations. The solid red line and the dashed blue line are guides for the eye with slopes $-36/11$ and -4, respectively. (b) PSD of 1D cuts $S_x(k)$ (blue diamonds, left axis) and $S_y(k)$ (red circles, right axis). The solid black line and the dashed green line are guides for the eye with slope $-27/11$ and $-25/9$, respectively. For visualization purposes, the values of $S(0,k)$ and $S_y(k)$ have been artificially offset vertically. All units are arbitrary.

Indeed, Eqs. (37)–(39) reduce to Eqs. (29)–(31) for $n = 1$ and $m = 2$. The advantage is that now we can make different choices for (n,m) in such a way that ζ is far from unity and SA behavior is enhanced. Note that a result such as Eqs. (37)–(39) is remarkable as it provides the solution for the scaling exponents of a two-parameter family of nonlinear equations. Actually, the symmetries leading to it circumvent the generation under renormalization of additional lower-order terms in the equation of motion, which would otherwise be expected. In principle, note that we have derived Eqs. (37)–(39) under the one-loop DRG approximation. An analogous result was obtained for the HK equation in [38,39], where it was argued to hold at any order in the DRG loop expansion. Again, it is due to the symmetries of the system as discussed above, leading to the three scaling relations among exponents. In the case of the HK equation proper, this even makes it possible to approximate it very accurately by a *linear* equation with the exact same scaling exponents [30].

As a specific example, we have performed numerical simulations of Eq. (33) with $n = 1/2$ and $m = 3$ in order to compare with the expected scaling exponents, which are

$$\alpha_x = \frac{9}{17}, \quad z_x = \frac{42}{17}, \quad \zeta = \frac{7}{17}. \tag{40}$$

The results, presented in Fig. 4 indeed agree with these values. Notice in this case full saturation of correlations along the y direction has not been achieved for our longest simulation times, hence the k_y-independent behavior of $S(0,k_y)$ and $S_y(k_y)$ at small arguments.

As a summary of the results in this section, we conclude that SA is indeed feasible for conserved equations with nonconserved noise which are invariant under global shifts of the height field. However, this requires the suppression of nonlinearities along one of the substrate directions, which is a nongeneric parameter condition. Notice, under such a constraint the equation cannot possibly be brought into

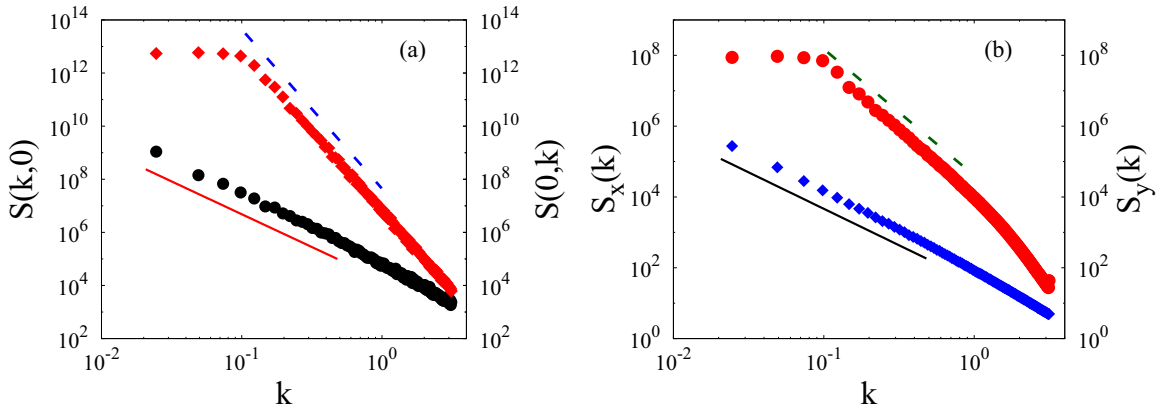

FIG. 4. (Color online) Numerical integrations of Eq. (33) for $n = 1/2$, $m = 3$, and parameters $\nu_x = \nu_y = 1$, $D = 1$, $\lambda_x = 2$, $L = 256$, $\Delta x = 1$, and $\Delta t = 0.05$. (a) One-dimensional projections $S(k,0)$ (black circles, left axis) and $S(0,k)$ (red diamonds, right axis) of the 2D PSD, averaged over 100 different noise realizations. The solid red line and the dashed blue line are guides for the eye with slopes $-42/17$ and -6, respectively. (b) PSD of 1D cuts $S_x(k)$ (blue diamonds, left axis) and $S_y(k)$ (red circles, right axis). The solid black line and the dashed green line are guides for the eye with slope $-35/17$ and $-25/7$, respectively. For visualization purposes, the values of $S(0,k)$ and $S_y(k)$ have been artificially offset vertically. All units are arbitrary.

isotropic form by any simple combination of coordinate rotations and/or rescalings in the substrate plane.

B. Systems without shift invariance: Generalized HK equation

As described in the Introduction, in our previous work [30] we considered the HK equation, which was originally proposed to describe the interface dynamics of a running-sandpile model in the context of SOC [38,39]. For a 2D substrate such as we are currently considering, this equation reads

$$\partial_t h = \nu_x \partial_x^2 h + \nu_y \partial_y^2 h - \frac{\lambda_x}{2}\partial_x h^2 + \eta. \tag{41}$$

In the original formulation [38,39], the linear terms model the relaxation of the height of the sand pile through diffusive transport, whereas the nonlinearity accounts for the lack of inversion symmetry in the x direction, being related to the presence of the external driving provided by the influx of sand. This is assumed to occur along the x axis, which is an example of a nongeneric condition for nonlinearities in the context of discussed in the previous section. The noise term η in Eq. (41) mimics the random addition of sand particles from outside the system, thus being nonconserved. This leads to GSI properties, in spite of the fact that the HK equation depends explicitly on h, and not only on its derivatives [11]. In particular, SA occurs, and scaling exponents have been obtained analytically in [38,39] through a DRG approach and numerically in [30], namely

$$\alpha_x^{\mathrm{HK}} = -\frac{1}{5}, \quad z_x^{\mathrm{HK}} = \frac{6}{5}, \quad \zeta^{\mathrm{HK}} = \frac{3}{5}. \tag{42}$$

Note that the negative values of $\alpha_{x,y}$ actually imply subdominant (logarithmic) behavior for observables in real space, such as, e.g., the surface roughness [6]. As discussed in detail in [30], they also lead to slow convergence even for observables in Fourier space, but which are integrals of the 2D PSD function, such as $S_{x,y}(k_{x,y})$. We meet again this type of behavior in some specific examples to be discussed below.

In view of the results of the previous section, a natural question is whether the different behavior of the HK equation under global shifts of the height, as compared to, e.g., the caKPZ equation, could allow for the occurrence of SA even for more generic parameter conditions such that, e.g., the nonlinear part of the equation could be brought into an isotropic form via appropriate coordinate transformations in the substrate plane. In order to elucidate this possibility, we generalize the HK equation into

$$\frac{\partial h}{\partial t} = \nu_x \partial_x^2 h + \nu_y \partial_y^2 h + \nu_{xy}\partial_x\partial_y h - \frac{\lambda_x}{2}\partial_x h^2 - \frac{\lambda_y}{2}\partial_y h^2 + \eta, \tag{43}$$

which is henceforth referred to as the gHK equation. Indeed, the original HK equation simply corresponds to the particular case of Eq. (43) in which $\lambda_x \neq 0$, while $\lambda_y = \nu_{xy} = 0$. The term proportional to ν_{xy} has been introduced for technical reasons, as becomes clear next.

In order to derive analytical insight into the critical behavior of the gHK equation, we apply to it the DRG procedure described in Sec. II. The flow equations for the renormalization of the parameters of the gHK equation read

$$\frac{d\nu_x}{dl} = \nu_x(z_x - 2 - \Sigma_{\nu_x}), \tag{44}$$

$$\frac{d\nu_{xy}}{dl} = \nu_{xy}(z_x - \zeta - 1 - \Sigma_{\nu_{xy}}), \tag{45}$$

$$\frac{d\nu_y}{dl} = \nu_y(z_x - 2\zeta - \Sigma_{\nu_y}), \tag{46}$$

$$\frac{d\lambda_x}{dl} = \lambda_x(\alpha_x + z_x - 1), \tag{47}$$

$$\frac{d\lambda_y}{dl} = \lambda_y(\alpha_x + z_x - \zeta), \tag{48}$$

$$\frac{dD}{dl} = D(z_x - 2\alpha_x - \zeta - 1), \tag{49}$$

where Σ_{ν_x}, Σ_{ν_y}, and $\Sigma_{\nu_{xy}}$ are functions of $\nu_{x,y}$ and $\lambda_{x,y}$, which are provided in Appendix A, together with further details on the derivation of Eqs. (44)–(49). From Eqs. (44)–(46) note that for the gHK equation, even if the term with bare parameter ν_{xy} were initially zero, it is, in principle, generated by the coarse-graining procedure. This is due to the fact that $\Sigma_{\nu_{xy}}$ has a prefactor of $1/\nu_{xy}$ [see Eq. (A30)], so that the term $\nu_{xy}\Sigma_{\nu_{xy}}$ in the flux equation for ν_{xy} will not generically vanish, even when $\nu_{xy} = 0$. This is the reason why we have incorporated it to the definition of Eq. (43) in order to correctly take it into account in the DRG analysis.

We can write an equivalent DRG flow which does not depend explicitly on α_x and z_x through the identification of natural couplings in the system, such as, e.g.,

$$g = \frac{\lambda_x^2 D}{16\pi^2\Lambda^2\nu_x^3}, \quad r_\nu = \frac{\nu_y}{\nu_x}, \quad f_\nu = \frac{\nu_{xy}}{\nu_x}, \quad r_\lambda = \frac{\lambda_y}{\lambda_x}. \tag{50}$$

Thus, we get

$$\frac{dr_\lambda}{dl} = r_\lambda(1 - \zeta), \tag{51}$$

$$\frac{df_\nu}{dl} = f_\nu\left[1 - \zeta + \Sigma_{\nu_x} - \Sigma_{\nu_{xy}}\right], \tag{52}$$

$$\frac{dr_\nu}{dl} = r_\nu\left[2(1 - \zeta) + \Sigma_{\nu_x} - \Sigma_{\nu_y}\right], \tag{53}$$

$$\frac{dg}{dl} = g\left[3 - \zeta + 3\,\Sigma_{\nu_x}\right]. \tag{54}$$

1. *HK equation as a particular case*

The behavior of the original HK equation, which corresponds to $r_\lambda = f_\nu = 0$, can be readily obtained from the above DRG results; see details in Appendix A 1 . The nontrivial part of the flow reduces in this case to

$$\frac{dr_\nu}{dl} = 2r_\nu(1 - \zeta) - g\left[\frac{3\zeta + (7 + \zeta)r_\nu + 5r_\nu^2}{(1 + r_\nu)^2} + 5\sqrt{r_\nu}\tan^{-1}(\sqrt{r_\nu}) + \frac{3\zeta}{\sqrt{r_\nu}}\tan^{-1}\left(\frac{1}{\sqrt{r_\nu}}\right)\right], \tag{55}$$

$$\frac{dg}{dl} = g(3 - \zeta) - \frac{3g^2}{r_\nu}\left[\frac{3\zeta + (7 + \zeta)r_\nu + 5r_\nu^2}{(1 + r_\nu)^2} + 5\sqrt{r_\nu}\tan^{-1}(\sqrt{r_\nu}) + \frac{3\zeta}{\sqrt{r_\nu}}\tan^{-1}\left(\frac{1}{\sqrt{r_\nu}}\right)\right]. \tag{56}$$

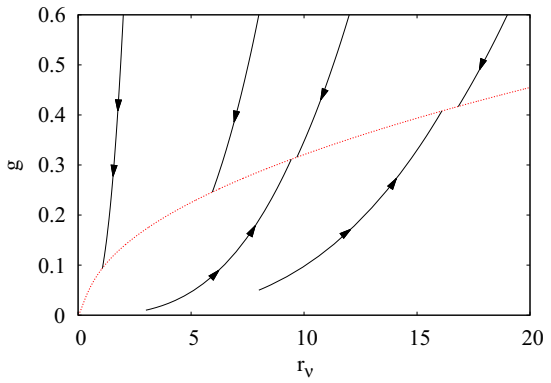

FIG. 5. (Color online) Numerical integration of the DRG flow for the gHK equation (43) in the HK limiting case $r_\lambda = f_v = 0$, Eqs. (53) and (54). The solid black lines are flow trajectories, while the dashed red line is the manifold of fixed points of the flow. All units are arbitrary.

The fixed points of Eq. (56) are either $g = 0$ or

$$g = g^* \equiv \frac{3-\zeta}{3} r_v \left[\frac{3\zeta + (7+\zeta) r_v + 5 r_v^2}{(1+r_v)^2} + 5\sqrt{r_v}\tan^{-1}(\sqrt{r_v}) + \frac{3\zeta}{\sqrt{r_v}} \tan^{-1}\left(\frac{1}{\sqrt{r_v}}\right)\right]^{-1}. \quad (57)$$

If $g = 0$, Eq. (53) implies $\zeta = 1$; see Eq. (55). In contrast, setting $g = g^*$ requires $\zeta = 3/5$ in order to yield a fixed point for Eqs. (53) and (54) [note that Eqs. (51) and (52) hold automatically since we have set $\nu_{xy} = \lambda_y = 0$]. Moreover, in this case a manifold of fixed points actually exists in (r_v, g) parameter space, described by the equation obtained once we set $\zeta = 3/5$ in Eq. (57), namely,

$$g = \frac{4}{5} r_v \left[\frac{9 + 38 r_v + 25 r_v^2}{5(1+r_v)^2} + 5\sqrt{r_v}\tan^{-1}(\sqrt{r_v}) + \frac{9}{5\sqrt{r_v}} \tan^{-1}\left(\frac{1}{\sqrt{r_v}}\right)\right]^{-1}. \quad (58)$$

In order to explore the stability of this family of fixed points, we have numerically integrated the flux (53) and (54) for $\nu_{xy} = \lambda_y = 0$. The result is shown in Fig. 5, where it is clear that all the fixed points on the manifold are attractive, illustrating how GSI occurs in this system. This is in stark contrast with the role of RG fixed points in equilibrium critical systems, which are unstable due to the relevance of temperature perturbations. Moreover, each point on the manifold corresponds to the *same* set of scaling exponents, which are obtained by going back to Eqs. (44)–(49), and plugging in the values of g^* and ζ. The resulting exponents have the expected values for the HK equation, namely Eq. (42).

2. *Full generalized HK equation*

In the case of the full gHK equation, it is clear from Eq. (51) that if $r_\lambda \neq 0$, then $\zeta = 1$ at the RG fixed point, leading to *isotropic asymptotic behavior*. In Appendix A 2, we explicitly provide the three remaining DRG flow equations, Eqs. (52)–(54) in this case. By numerically exploring the parameter space, for $0.3 \leqslant r_\lambda \leqslant 1.2$ we have found a nontrivial manifold of fixed points, which can actually be seen as a line parametrized by the value of r_λ. All points on this manifold share the scaling exponents values

$$\alpha_x = -\frac{1}{3}, \quad z_x = \frac{4}{3}, \quad \zeta = 1. \quad (59)$$

In Fig. 6 we show the numerical integration of the DRG flow for r_λ within this range. Similar considerations can be made as those provided for Fig. 5.

However, we have not been able to find a similar set of fixed points for other values of r_λ. Due to the strong nonlinear character of the equations that one needs to solve (see Appendix A), it is uncertain whether this is due to lack of convergence of the numerical scheme we have employed to integrate the DRG flow equations or to an artifact of the approximations made within our DRG approach itself. Nevertheless, one would expect such fixed points to also exist and correspond to exponent values as given in Eq. (59). In order to verify this conjecture, we have performed direct numerical simulations of the full gHK equation using the

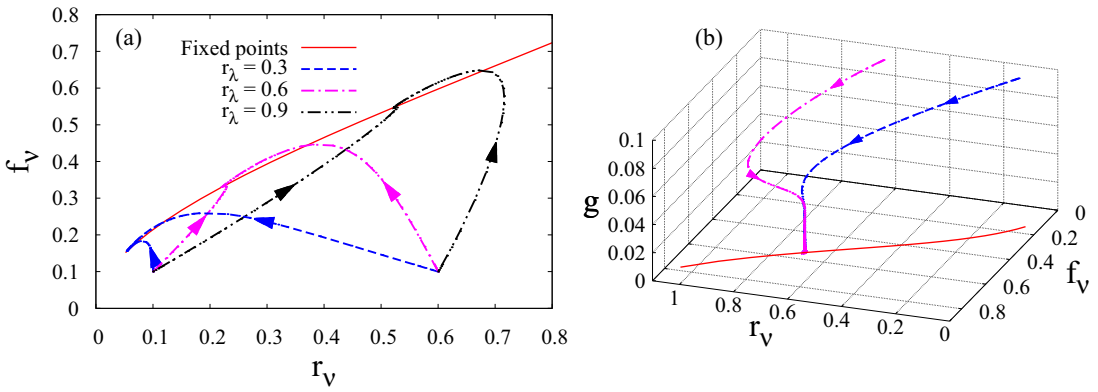

FIG. 6. (Color online) Numerical integration of the DRG flow for the gHK equation (43) in the case $\zeta = 1$ [Eqs. (52)–(54)]. (a) Projection on the (r_v, f_v) plane for two initial conditions, $(r_v, f_v, g) = (0.1, 0.1, 0.1)$ and $(0.6, 0.1, 0.1)$, and several values of r_λ in each case, as indicated in the legend. The solid red line is the manifold of fixed points, parametrized by r_λ. (b) Three-dimensional view of two flow trajectories for $r_\lambda = 1$ and the same two initial conditions as in the left panel. Again, the solid red line is the manifold of fixed points. All units are arbitrary.

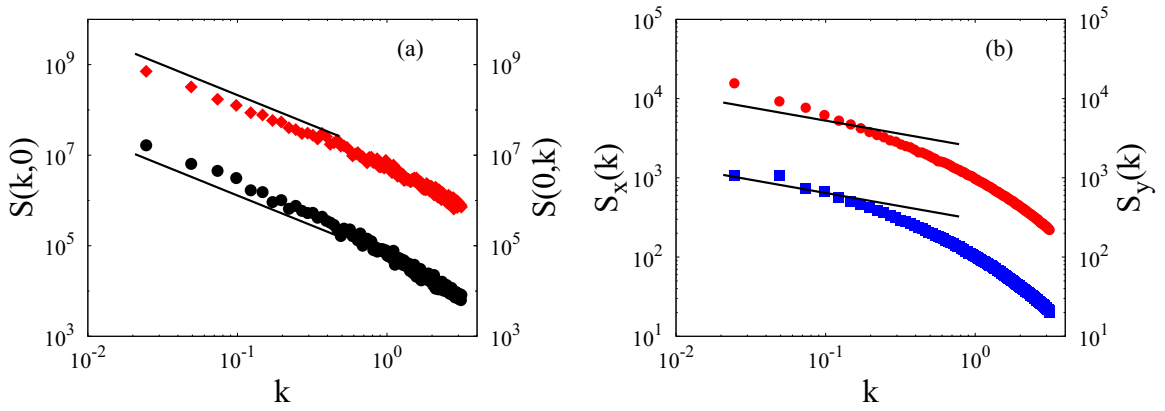

FIG. 7. (Color online) Numerical integrations of the gHK equation [Eq. (43)] for parameters $\nu_x = \nu_y = 1, \nu_{xy} = 0, D = 1, \lambda_x = 1, \lambda_y = -2$ (so that $r_\lambda < 0$), $L = 256$, $\Delta x = 1$, and $\Delta t = 0.01$. (a) One-dimensional projections $S(k,0)$ (black circles, left axis) and $S(0,k)$ (red diamonds, right axis), averaged over 50 different noise realizations. The solid black lines are guides for the eye with slope $-4/3$. (b) PSD of 1D cuts $S_x(k)$ (blue squares, left axis) and $S_y(k)$ (red circles, right axis). The solid black lines are guides for the eye with slope $-1/3$. For visualization purposes, the values of $S(0,k)$ and $S_y(k)$ have been artificially offset vertically. All units are arbitrary.

same pseudospectral scheme as above. We have paid particular attention to a potential change of scaling behavior due to a relative change in the signs of the nonlinearities λ_x and λ_y. As is clear from the left panels of Figs. 7 and 8, in the hydrodynamic limit the equation displays the expected isotropic exponent values [Eq. (59)], irrespective of such a relative sign, analogous in this sense to the caKPZ equation.

Looking at the right panels of Figs. 7 and 8, the analytical predictions for the 1D PSDs apparently do not agree with the results from numerical simulations. A very similar phenomenon has been found and studied for the HK equation in [30, Figs. 9 through 11]. In that case, the discrepancy was due to finite size effects for the system sizes employed in the numerical simulation of the equation, and we believe that a similar phenomenon is taking place here. It is worth mentioning that such a lack of convergence seems more pronounced for the PSD of cuts along the y direction than for cuts along the x direction, probably related with the value of λ_y, which is larger in absolute value than λ_x in both cases.

IV. NONCONSERVED DYNAMICS

After the previous results, it is natural to ponder whether strongly anisotropic behavior can actually occur for GSI systems with nonconserved dynamics. The prime representative of them is the aKPZ equation [18], namely,

$$\partial_t h = \nu_x \partial_x^2 h + \nu_y \partial_y^2 h + \frac{\lambda_x}{2}(\partial_x h)^2 + \frac{\lambda_y}{2}(\partial_y h)^2 + \eta. \qquad (60)$$

This equation was studied in detail in the seminal paper [18]. The main result was that the scaling behavior is always isotropic, changing from linear Edwards-Wilkinson (EW) type to nonlinear KPZ type as a function of the nonlinearities having opposite or the same signs, respectively. However, the case in which only one of the nonlinearities is zero remained basically unexplored. Our results above suggest that it might lead to SA behavior, and for this reason we revisit the DRG analysis in [18], complementing it with direct numerical simulations of the equation. Moreover, while detailed calculations are

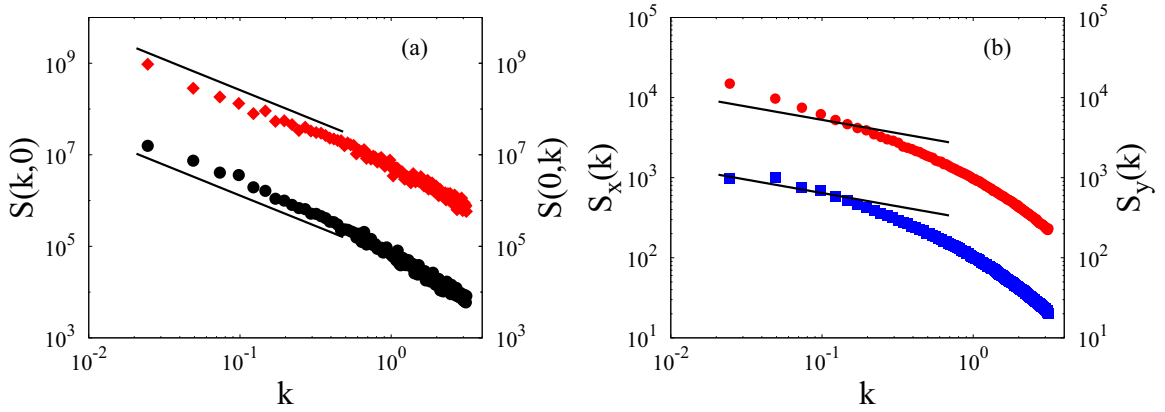

FIG. 8. (Color online) Numerical integrations of the gHK equation [Eq. (43)] for parameters $\nu_x = \nu_y = 1, \nu_{xy} = 0, D = 1, \lambda_x = 1, \lambda_y = 2$ (so that $r_\lambda > 0$), $L = 256$, $\Delta x = 1$, and $\Delta t = 0.01$. (a) One-dimensional projections $S(k,0)$ (black circles, left axis) and $S(0,k)$ (red diamonds, right axis) of the 2D PSD, averaged over 50 different noise realizations. The solid black lines are guides for the eye with slope $-4/3$. (b) PSD of 1D cuts $S_x(k)$ (blue squares, left axis) and $S_y(k)$ (red circles, right axis). The solid black lines are guides for the eye with slope $-1/3$. For visualization purposes, the values of $S(0,k)$ and $S_y(k)$ have been artificially offset vertically. All units are arbitrary.

available for the caKPZ system [20], this is not the case of Eq. (60). For this reason we provide details on our analysis in Appendix B.

DRG analysis of the anisotropic KPZ equation

In the case of Eq. (60), the DRG flow equations read, in general,

$$\frac{d\nu_x}{dl} = \nu_x\left(z_x - 2 - \Sigma_{\nu_x}\right), \tag{61}$$

$$\frac{d\nu_y}{dl} = \nu_y\left(z_x - 2\zeta - \Sigma_{\nu_y}\right), \tag{62}$$

$$\frac{d\lambda_x}{dl} = \lambda_x(z_x + \alpha_x - 2), \tag{63}$$

$$\frac{d\lambda_y}{dl} = \lambda_y(z_x + \alpha_x - 2\zeta), \tag{64}$$

$$\frac{dD}{dl} = D(z_x - 2\alpha_x - \zeta - 1 + \Phi_D), \tag{65}$$

where functions Σ_{ν_x}, Σ_{ν_y}, and Φ_D are reported in Appendix B, together with the main steps in their calculation. From Eqs. (63) and (64) we immediately see that, if both nonlinearities are nonzero, $\lambda_x\lambda_y \neq 0$, a fixed point can be attained only for a weakly anisotropic system, which is $\zeta = 1$. By introducing the couplings

$$r_\nu = \frac{\nu_y}{\nu_x}, \qquad r_\lambda = \frac{\lambda_y}{\lambda_x}, \qquad g = \frac{\lambda_x^2 D}{32\pi^2\nu_x^3}, \tag{66}$$

we again obtain a renormalization flow that is independent of α_x and z_x, specifically,

$$\frac{dr_\nu}{dl} = 2r_\nu(1-\zeta)\left\{1 - g\left[\frac{3+r_\nu}{(1+r_\nu)^2} - A_{\zeta,r_\nu} + \frac{r_\lambda}{r_\nu}\left(\frac{4}{1+r_\nu} + \frac{r_\lambda}{r_\nu}\left(A_{\zeta,r_\nu} + \frac{1+3r_\nu}{(1+r_\nu)^2}\right)\right)\right]\right\}, \tag{67}$$

$$\frac{dr_\lambda}{dl} = 2r_\lambda(1-\zeta), \tag{68}$$

$$\frac{dg}{dl} = g(1-\zeta)\left\{1 - g\left[\frac{13+3r_\nu}{(1+r_\nu)^2} - 3A_{\zeta,r_\nu} + \frac{r_\lambda}{r_\nu}\left(8A_{\zeta,r_\nu} + 8\frac{2r_\nu+1}{(1+r_\nu)^2} + \frac{r_\lambda}{r_\nu}\left(3A_{\zeta,r_\nu} + \frac{3+5r_\nu}{(1+r_\nu)^2}\right)\right)\right]\right\}, \tag{69}$$

where we have introduced the auxiliary function (proportional to the one defined in [18])

$$A_{\zeta,r_\nu} = \frac{\tan^{-1}(\sqrt{r_\nu}) + \zeta\tan^{-1}(\sqrt{1/r_\nu})}{(\zeta-1)\sqrt{r_\nu}}. \tag{70}$$

Without loss of generality, we can consider only the cases $r_\lambda \neq 0$ and $r_\lambda = 0$ (a zero λ_x, i.e., $r_\lambda = \infty$, is not taken into account due to the symmetry of the aKPZ equation with respect to an exchange in the spatial coordinates $x \leftrightarrow y$). For $r_\lambda \neq 0$, the fixed points of the set of Eqs. (67)–(69) must satisfy the condition $\zeta = 1$ (WA), the only terms different from zero being those proportional to $(1-\zeta)A_{1,r_\nu} = -\pi/2\sqrt{r_\nu}$, so that the nontrivial part of the flow (67)–(69) becomes

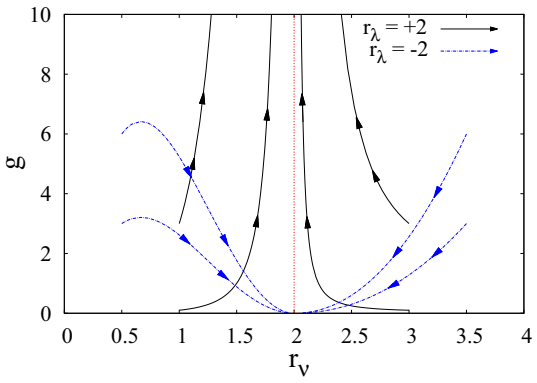

FIG. 9. (Color online) Numerical intergation of the DRG Flow for the aKPZ equation (60) for the case $\zeta = 1$ [Eqs. (71) and (72)]. The solid black lines correspond to the case of positive r_λ, while the dashed blue lines correspond to $r_\lambda < 0$.

$$\frac{dr_\nu}{dl} = g\pi\sqrt{r_\nu}\left[\left(\frac{r_\lambda}{r_\nu}\right)^2 - 1\right], \tag{71}$$

$$\frac{dg}{dl} = 4\pi\frac{g^2}{\sqrt{r_\nu}}\left\{\frac{r_\lambda}{r_\nu} + \frac{3}{8}\left[\left(\frac{r_\lambda}{r_\nu}\right)^2 - 1\right]\right\}. \tag{72}$$

The fixed points of this set of equations need to belong to the manifold $(r_\nu^*, r_\lambda^*, g^*, \zeta) = (r_\nu, r_\lambda, 0, 1)$, with $r_\nu > 0$. Beyond the trivial solution $(0, r_\lambda, 0, 1)$ (see below), which corresponds to EW behavior, two submanifolds of $(r_\nu, r_\lambda, 0, 1)$ provide nontrivial fixed points. Indeed, by equating (71) to zero we have $r_\lambda = \pm r_\nu$ and fixed points $(r_\nu, \pm r_\nu, 0, 1)$, while from Eq. (72) we obtain the two solutions $r_\lambda = r_\nu/3, -3r_\nu$, i.e., $(r_\nu, r_\nu/3, 0, 1)$ and $(r_\nu, -3r_\nu, 0, 1)$. Nevertheless, difficulties arise when we try to compute the stability of these points. In fact, the stability matrix has three elements equal to zero for $g = 0$. Even though a more refined analysis is possible, the RG flow can be more conveniently studied through numerical integration of Eqs. (71) and (72). In Fig. 9 we show results of such a study. If we take a bare parameter condition such that $r_\lambda < 0$ (dashed blue lines), the flow is attracted by the fixed point at the origin, namely, scaling behavior is WA and linear, scaling exponents being those of the EW equation in $2+1$ dimensions, namely, $\alpha_x = \alpha_y = 0$ (logarithmic) and $z_x = z_y = 2$ [6]. In contrast, for bare parameter choices such that $r_\lambda > 0$ (solid black lines in Fig. 9) the RG flow lines move towards unbounded values for g. This is a manifestation of the occurrence of WA nonlinear KPZ scaling, which is well known not to lead to a finite fixed point in $2+1$ dimensions [6]. Thus, as expected, Wolf's results are recovered through the numerical integration of the RG flow.

Once the well-known results for the aKPZ equation have been retrieved, we focus next on the case of SA $\zeta \neq 1$. From Eq. (68) we immediately obtain $r_\lambda = 0$ at the fixed points, so that the DRG flow equations reduce to

$$\frac{dr_\nu}{dl} = 2r_\nu(1-\zeta)\left\{1 - g\left[\frac{3+r_\nu}{(1+r_\nu)^2} - A_{\zeta,r_\nu}\right]\right\}, \tag{73}$$

$$\frac{dg}{dl} = g(1-\zeta)\left\{1 - g\left[\frac{13+3r_\nu}{(1+r_\nu)^2} - 3A_{\zeta,r_\nu}\right]\right\}. \tag{74}$$

In order to find the fixed points for Eqs. (73) and (74), we need to set their right-hand sides to zero. This gives us several possible solutions, which we proceed to analyze. Considering Eq. (73), zeros are obtained setting $r_\nu = r_\nu^* = 0$ or $g = g_1^* = [(3+r_\nu)(1+r_\nu)^{-2} - A_{\zeta,r_\nu}]^{-1}$.

However, the following should also be considered.

(a) When $r_\nu = 0$, Eq. (74) cannot be set to zero. This is due to the fact that one of the terms within the equation, namely, $g^2[\tan^{-1}(r_\nu^{1/2}) + \zeta \tan^{-1}(r_\nu^{-1/2})]r_\nu^{-1/2}$, does not have a well defined limit as a two-variable function for $(r_\nu, g) \to (0,0)$.

(b) Substituting g_1^* into Eq. (74), we get

$$A_{\zeta,r_\nu} = \frac{5+r_\nu}{(1+r_\nu)^2}, \tag{75}$$

which gives us the possible values of r_ν and ζ corresponding to g_1^*. However, it is not difficult to see that Eq. (75) leads to $g_1^* = -(1+r_\nu)^2/2 < 0$, which is not a physically acceptable value.

Hence, the formal zeros of Eq. (73) provided by $r_\nu = 0$ and $g = g_1^*$ are both to be discarded. On the other hand, if we start out with Eq. (74), we obtain zeros for $g = 0$ and $g = g_2^* = [(13+3r_\nu)(1+r_\nu)^{-2} - 3A_{\zeta,r_\nu}]^{-1}$. Then we get the following.

(a) By substituting $g = 0$ into Eq. (73) we get

$$\frac{dr_\nu}{dl} = 2r_\nu(1-\zeta), \tag{76}$$

which implies that the line $g = 0, r_\nu > 0$ is a separatrix for the RG flow. One could then argue that the point $g = 0, r_\nu = 0$ is indeed a fixed point, but strictly speaking this is not true due to the ill-definiteness of the flow at the origin, as discussed above.

(b) If we substitute $g = g_2^*$ into Eq. (73), we again obtain Eq. (75) and therefore no physically acceptable fixed points.

A final possibility to find a meaningful fixed point of the flow is to set $\zeta = 1$, which would correspond to isotropic asymptotic behavior. Equations (73) and (74) then become

$$\frac{dr_\nu}{dl} = -\pi g\sqrt{r_\nu}, \tag{77}$$

$$\frac{dg}{dl} = -\frac{3\pi}{2}\frac{g^2}{\sqrt{r_\nu}}. \tag{78}$$

As it turns out, these equations can be exactly solved, giving

$$r_\nu(l) = \frac{r_0^{3/2}}{\sqrt{r_0} + \pi g_0 l}, \tag{79}$$

$$g(l) = \frac{g_0 r_0^{3/4}}{(\sqrt{r_0} + \pi g_0 l)^{3/2}}, \tag{80}$$

where $r_0 = r_\nu(0)$ and $g_0 = g(0)$ are the initial conditions (bare parameter values). This exact solution tells us that the flow moves towards the point $r_\nu = 0$, $g = 0$, which is only reached in infinite "time," i.e., for $l \to \infty$. Moreover, Eqs. (79) and (80) can be simply restated as

$$g(l) = g_0\left[\frac{r_\nu(l)}{r_0}\right]^{3/2}, \tag{81}$$

implying that g vanishes faster than r_ν in this limit.

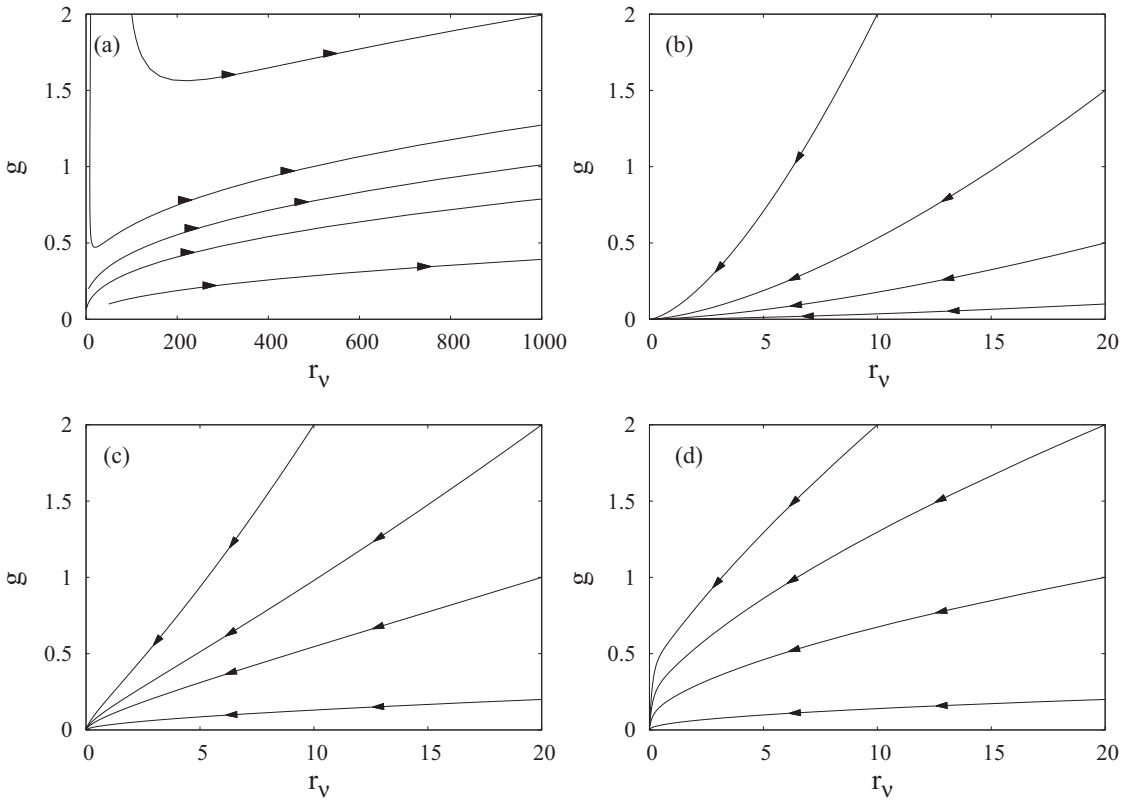

FIG. 10. Numerical integration of the DRG flow for the aKPZ equation (60) for the case $r_\lambda = 0$ [Eqs. (73) and (74)] and different values of the anisotropy exponent, (a) $\zeta = 1/2$, (b) $\zeta = 1$, (c) $\zeta = 3/2$, and (d) $\zeta = 5$. All units are arbitrary.

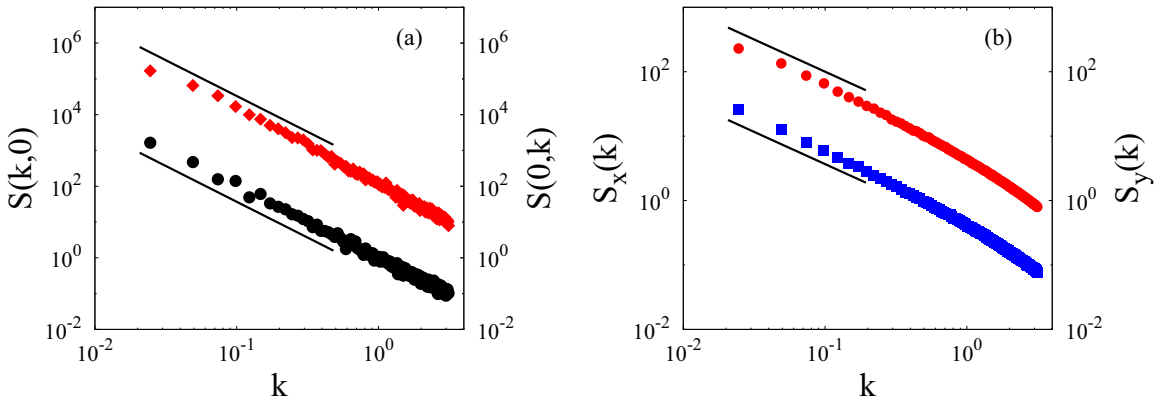

FIG. 11. (Color online) Numerical integrations of the aKPZ equation [Eq. (60)] for parameters $\nu_x = \nu_y = 1$, $D = 1$, $\lambda_x = 3$, $\lambda_y = 0$, $L = 256$, $\Delta x = 1$, and $\Delta t = 0.01$. (a) One-dimensional projections $S(k,0)$ (black circles, left axis) and $S(0,k)$ (red diamonds, right axis), averaged over 50 different noise realizations. The solid black lines are guides for the eye with slope -2. (b) PSD of 1D cuts along the x direction, $S_x(k)$ (blue squares, left axis), and along the y direction, $S_y(k)$ (red circles, right axis). The solid black lines are guides for the eye with slope -1. For visualization purposes, the values of $S(0,k)$ and $S_y(k)$ have been artificially offset vertically. All units are arbitrary.

The latter result actually allows us to rationalize the behavior of the RG flow [Eqs. (67)–(69)] for the anisotropic condition $\zeta \neq 1$, $r_\lambda = 0$, as obtained through numerical integration of the corresponding Eqs. (73) and (74). In Fig. 10 we show such type of results for different values of ζ. Obviously, $\zeta = 1$ [see Fig. 10(b)] constitutes a natural reference case for which, as we have just seen, the RG flow is both well defined at, and attracted by, the origin, where scaling behavior is isotropic, EW type. Even though this point cannot be reached by the RG flow at finite l for other values of ζ, for which no finite fixed points otherwise exist, it still plays an important role. Thus, as can be seen in Fig. 10(a), for $\zeta < 1$ the origin seems to repel the flow lines, which evolve towards arbitrarily large values of (r_ν, g). This behavior may be an artifact of the approximations made in the DRG analysis, as suggested by further results. Namely, $\zeta > 1$ is seen in Figs. 10(c) and 10(d) to reverse the stability of the origin. Now it attracts the RG trajectories, which flow into it for infinite l, indicating asymptotic isotropic EW behavior. We have checked that it is the latter behavior, rather than the unbounded growth of r_ν and g obtained for $\zeta < 1$, which seems to actually occur for the aKPZ equation under the present type of conditions. Specifically, we have performed direct numerical simulations of the aKPZ equation [Eq. (60)] for a case in which one of the nonlinearities is "suppressed," $\lambda_y = 0$; see Fig. 11 [52]. As can be seen in the figures, the behavior of correlation functions is well reproduced by isotropic EW exponents, namely, $\alpha = 0$ (logarithmic) and $z = 2$. This is consistent with the effective g coupling renormalizing to zero much faster than r_ν, so that at large length scales the system is effectively behaving as an anisotropic EW equation, for which the scaling is well known to be of the WA type [30].

V. CONCLUSIONS AND OUTLOOK

The previous sections have allowed us to assess the nongenericity of SA for surfaces displaying GSI and nonlinear effects. Thus, for nonconserved dynamics, SA simply does not occur, even for special conditions under which only one of the nonlinearities is suppressed. On the other hand, for systems with conserved dynamics, SA can be obtained, and even whole families of equations can be formulated which display this property, such as Eq. (33). However, both in the presence and in the absence of the shift symmetry $h \to h + \text{const.}$, this seems only possible for "incomplete" equations in which only one of the nonlinearities is suppressed.

Overall, for the type of systems that we have studied here and in [30], one can conclude that, if the part of the interface equation which is most relevant for the scaling behavior (e.g., nonlinear vs linear terms, or surface tension vs surface diffusion, etc.) can be rewritten in an isotropic form using coordinate transformations, such as rotations or a mere rescaling (in which rescaling factors are *positive*), then the system will display *WA*. Actually, this is a sufficient condition for WA, but is not necessary: One also obtains WA for example in the aKPZ equation when the coefficients of the nonlinearities have different signs. Note that a rescaling in such a situation still preserves the difference in sign between the two nonlinear terms.

However, in order to obtain SA, one further needs conserved dynamics, combined with special parameter cancellations such that, e.g., $\lambda_x \neq 0$, while $\lambda_y = 0$. In general, conditions of this type depend critically on details of the dynamics that is being described, acting as special constraints, and are in this sense nongeneric in parameter space. Hence, they can be overlooked by simple-minded derivations of the equations of motion based on symmetries and conservation laws.

Naturally, there are formulations of the interface equation, such as the original one by HK, in which this type of special conditions becomes natural, as imposed by the geometry of the external driving fields and/or relaxation mechanisms (e.g., the direction of sand transport, etc.). Beyond driven diffusive systems or models of SOC, such constraints also appear, for instance, in solidification fronts [53], the dynamics of localized structures [54] in plasmas [55] and in fluid propagation [56], the evolution of driven flux lines in superconductors [57], or the effect of shear on interface fluctuations [58]. Still, such constraints leading to "incomplete" equations are not to be expected in many other systems. Consider, for instance, epitaxial growth systems [18,59] in which lattice anisotropies are expected to lead to different values of, say, λ_x and λ_y. In general, the physics is limited to inducing different

values in the equation parameters, but not necessarily to exact cancellations of specific ones.

We have to note an additional (implicit) assumption that we have made in our analysis. This is the fact that the interface equation is morphologically stable, in the sense that the deterministic terms tend to smooth out surface inhomogeneities. However, many natural contexts for the occurrence of spatial anisotropies are actually systems in which patterns emerge (convection rolls, ripples under IBS, etc.), some of which correspond to references just cited [53–56,59]. Formation of this type of structures requires morphological instabilities to occur, which suggests pattern-forming systems as a potential context for nontrivial strongly anisotropic behavior. Note that pattern-forming behavior (i.e., the emergence of a spatial structure from an homogeneous system) is to some extent the converse interfacial property to GSI, since the former is characterized by the predominance of a characteristic length scale (namely, the pattern periodicity), which is absent in the latter. Nevertheless, studies are already available [48,49] in which a highly nontrivial interplay occurs between instability and anisotropy, and in which the difference between scale invariance (kinetic roughening, or surface GSI) and its opposite property (pattern formation) is a matter of space and time scales [60,61]. The anisotropic Kuramoto-Sivashinsky equation [48,49,59,62] is a natural example, albeit itself being possibly confined to WA. Thus, we believe an interesting avenue for further studies of the occurrence of SA in generic scale-invariant systems is related with anisotropic models of pattern formation that are compatible with kinetic roughening at the appropriate scales.

ACKNOWLEDGMENTS

Partial support for this work has been provided by MINECO (Spain) Grant No. FIS2012-38866-C05-01. E.V. acknowledges support by Universidad Carlos III de Madrid.

APPENDIX A: DYNAMIC RENORMALIZATION GROUP ANALYSIS OF THE GENERALIZED HWA-KARDAR EQUATION

The diagrammatic expansion of the integrals that contribute to the renormalization of the bare propagator of the gHK equation is sketched in Fig. 12, where we use standard notation for the nonlinearities involved [43]. Note that, there being two different vertices with couplings $\lambda_{x,y}$, both indices l,m take as values the two spatial variables x,y, leading to four different contributions, Σ_{xx}, Σ_{xy}, Σ_{yx}, and Σ_{yy}.

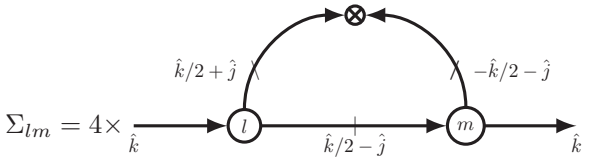

FIG. 12. Generic diagrammatic representation of the four different contributions Σ_{xx}, Σ_{xy}, Σ_{yx}, and Σ_{yy} to the renormalization of the propagator $G(\mathbf{k},\omega)$ of the gHK and the aKPZ equations. For each equation the exact meaning of the solid lines differ; see Eq. (A1) for the former and Eq. (B1) for the latter.

After the usual symmetrization of the integration variables $(\mathbf{q},\Omega) \to (\mathbf{j}+\mathbf{k}/2,\Omega+\omega/2)$, we get

$$\Sigma_{lm}(\mathbf{k},\omega) = -2\lambda_l\lambda_m D \int^{>} \frac{d\mathbf{j}}{(2\pi)^2} \int \frac{d\Omega}{2\pi} k_l \left(\frac{k_m}{2} - j_m\right) \times \left|G_0\left(\frac{\hat{k}}{2}+\hat{j}\right)\right|^2 G_0\left(\frac{\hat{k}}{2}-\hat{j}\right), \tag{A1}$$

where $G_0(\hat{k})$ is shorthand notation for the bare propagator

$$G_0(\hat{k}) = \left[\nu_x k_x^2 + 2\nu_{xy}k_xk_y + \nu_y k_y^2 - i\omega\right]^{-1}. \tag{A2}$$

An expansion to first order in $k_x/j_x, k_y/j_y \ll 1$ leads to

$$\lim_{\omega\to 0} |G_0(\hat{k}/2+\hat{j})|^2 \sim \frac{1}{\Delta^2+\Omega^2}\left[1 - \frac{2\Delta}{\Delta^2+\Omega^2}(\nu_x j_x k_x + \nu_y j_y k_y + \nu_{xy} j_y k_x + \nu_{xy} j_x k_y)\right], \tag{A3}$$

$$\lim_{\omega\to 0} G_0(\hat{k}/2-\hat{j}) \sim \frac{1}{\Delta+i\Omega}\left[1 + \frac{1}{\Delta+i\Omega}(\nu_x j_x k_x + \nu_y j_y k_y + \nu_{xy} j_y k_x + \nu_{xy} j_x k_y)\right], \tag{A4}$$

where $\Delta = \nu_x j_x^2 + 2\nu_{xy} j_x j_y + \nu_y j_y^2$. Using these results in Eq. (A1) and after integration over the frequency variable Ω, we retain terms up to second order in the components of $\mathbf{k}$, to get

$$\Sigma_{lm}(\mathbf{k},0) = -\frac{\lambda_l\lambda_m D}{16\pi^2} \int^{>} \frac{d\mathbf{j}}{\Delta^2}\left[k_l k_m + \frac{2}{\Delta} k_l j_m \times (\nu_x k_x j_x + \nu_y k_y j_y + \nu_{xy} j_y k_x + \nu_{xy} j_x k_y)\right]. \tag{A5}$$

Considering all possible combinations for $l,m = x,y$, we obtain the coarse-grained propagator, $\Sigma = \Sigma_{xx} + \Sigma_{xy} + \Sigma_{yx} + \Sigma_{yy}$, where

$$\Sigma_{xx}(\mathbf{k},0) = -\frac{\lambda_x^2 D}{16\pi^2} \int^{>} \frac{d\mathbf{j}}{\Delta^2}\left\{\left[1 + \frac{2}{\Delta}\left(\nu_x j_x^2 + \nu_{xy} j_x j_y\right)\right]k_x^2 + \frac{2}{\Delta}\left(\nu_y j_x j_y + \nu_{xy} j_x^2\right)k_x k_y\right\}, \tag{A6}$$

$$\Sigma_{xy}(\mathbf{k},0) = -\frac{\lambda_x\lambda_y D}{16\pi^2} \int^{>} \frac{d\mathbf{j}}{\Delta^2}\left\{\frac{2}{\Delta}\left(\nu_x j_x j_y + \nu_{xy} j_y^2\right)k_x^2 + \left[1 + \frac{2}{\Delta}\left(\nu_y j_y^2 + \nu_{xy} j_x j_y\right)\right]k_x k_y\right\}, \tag{A7}$$

$$\Sigma_{yx}(\mathbf{k},0) = -\frac{\lambda_x\lambda_y D}{16\pi^2} \int^{>} \frac{d\mathbf{j}}{\Delta^2}\left\{\frac{2}{\Delta}\left(\nu_y j_x j_y + \nu_{xy} j_x^2\right)k_y^2 + \left[1 + \frac{2}{\Delta}\left(\nu_x j_x^2 + \nu_{xy} j_x j_y\right)\right]k_x k_y\right\}, \tag{A8}$$

$$\Sigma_{yy}(\mathbf{k},0) = -\frac{\lambda_y^2 D}{16\pi^2} \int^{>} \frac{d\mathbf{j}}{\Delta^2}\left\{\left[1 + \frac{2}{\Delta}\left(\nu_y j_y^2 + \nu_{xy} j_x j_y\right)\right]k_y^2 + \frac{2}{\Delta}\left(\nu_x j_x j_y + \nu_{xy} j_y^2\right)k_x k_y\right\}. \tag{A9}$$

The next step is to calculate the **k** contributions to these integrals induced by the dependence on the wave-vector components of the integration limits that define the rectangular momentum shell which is being integrated out. Due to the lack of symmetry of the function Δ with respect to j_x and j_y, we cannot use only the first quadrant of the momentum shell to find them. Rather, it is convenient to expand Eqs. (A6)–(A9) in the limit $\delta l \to 0$. This allows us to rewrite each contribution Σ_{lm} to the renormalization of the propagator in a simpler form. In fact, for any function $f(j_x,j_y)$ appearing in the integrand of Eq. (A5), its integral decomposes into four terms, namely,

$$\int^{>} d\mathbf{j}\, f(j_x,j_y) = \int_{\Lambda/b}^{\Lambda} dj_x\, f_x(j_x) + \int_{-\Lambda}^{-\Lambda/b} dj_x\, f_x(j_x) + \int_{\Lambda/b^\zeta}^{\Lambda} dj_y\, f_y(j_y) + \int_{-\Lambda}^{-\Lambda/b^\zeta} dj_y\, f_y(j_y), \tag{A10}$$

where the associated single-variable functions f_x and f_y are simply given by

$$f_x(j_x) = \int_{-\Lambda}^{\Lambda} ds\, f(j_x,s), \tag{A11}$$

$$f_y(j_y) = \int_{-\Lambda}^{\Lambda} ds\, f(s,j_y). \tag{A12}$$

By expanding perturbatively Eq. (A10) for $b = e^{\delta l} \to 1$ we obtain the general result

$$\int^{>} d\mathbf{j}\, f(j_x,j_y) \sim [f_x(\Lambda) + f_x(-\Lambda) + \zeta f_y(\Lambda) + \zeta f_y(-\Lambda)]\Lambda\, \delta l. \tag{A13}$$

For the specific functions appearing in Eq. (A5), it is easy to verify that $f_{x,y}(\Lambda) = f_{x,y}(-\Lambda)$, so that, in this particular case,

$$\int^{>} d\mathbf{j}\, f(j_x,j_y) \sim 2[f_x(\Lambda) + \zeta f_y(\Lambda)]\Lambda\, \delta l. \tag{A14}$$

Then it is convenient to express the general contribution to the coarse-grained propagator as

$$\Sigma_{lm}(\mathbf{k},0) = -\frac{\lambda_l\lambda_m D}{8\pi^2}\left[\int_{-\Lambda}^{\Lambda} ds\, \frac{N_{lm}(\Lambda,s)}{\Delta_y^3(s)} + \zeta\int_{-\Lambda}^{\Lambda} ds\, \frac{N_{lm}(s,\Lambda)}{\Delta_x^3(s)}\right]\Lambda\delta l, \tag{A15}$$

where

$$\Delta_x(s) = \Delta(s,\Lambda) = \nu_x s^2 + 2\nu_{xy}\Lambda s + \nu_y\Lambda^2, \tag{A16}$$

$$\Delta_y(s) = \Delta(\Lambda,s) = \nu_x\Lambda^2 + 2\nu_{xy}\Lambda s + \nu_y s^2, \tag{A17}$$

$$N_{lm}(j_x,j_y) = (\nu_x j_x^2 + 2\nu_{xy} j_x j_y + \nu_y j_y^2)k_l k_m + 2(\nu_x j_x j_m + \nu_{xy} j_y j_m)k_l k_x + 2(\nu_y j_y j_m + \nu_{xy} j_x j_m)k_l k_y. \tag{A18}$$

Only six integrals need to be evaluated in order to cast Eq. (A15) into a form that can be used in our further analysis, namely,

$$J_i^x = \int_{-\Lambda}^{\Lambda} ds\, s^i/\Delta_x^3(s), \tag{A19}$$

$$J_i^y = \int_{-\Lambda}^{\Lambda} ds\, s^i/\Delta_y^3(s), \tag{A20}$$

for $i = 0,1,2$. At this stage of the calculation it is practical to leave them unspecified; hence,

$$\Sigma_{xx}(\mathbf{k},0) = -\frac{\lambda_x^2 D\Lambda}{8\pi^2}\{[3\nu_x(\zeta J_2^x + \Lambda^2 J_0^y) + 4\nu_{xy}\Lambda(\zeta J_1^x + J_1^y) + \nu_y(\zeta\Lambda^2 J_0^x + J_2^y)]k_x^2 + 2[\nu_{xy}(\zeta J_2^x + \Lambda^2 J_0^y) + \nu_y\Lambda(\zeta J_1^x + J_1^y)]k_x k_y\}\delta l, \tag{A21}$$

$$\Sigma_{xy}(\mathbf{k},0) = -\frac{\lambda_x\lambda_y D\Lambda}{8\pi^2}\{[\nu_x(\zeta J_2^x + \Lambda J_0^y) + 4\nu_{xy}\Lambda(\zeta J_1^x + J_1^y) + 3\nu_y(\zeta\Lambda^2 J_0^x + J_2^y)]k_x k_y + 2[\nu_{xy}(\zeta\Lambda^2 J_0^x + J_2^y) + \nu_x\Lambda(\zeta J_1^x + J_1^y)]k_x^2\}\delta l, \tag{A22}$$

$$\Sigma_{yx}(\mathbf{k},0) = -\frac{\lambda_x\lambda_y D\Lambda}{8\pi^2}\{[3\nu_x(\zeta J_2^x + \Lambda^2 J_0^y) + 4\nu_{xy}\Lambda(\zeta J_1^x + J_1^y) + \nu_y(\zeta\Lambda^2 J_0^x + J_2^y)]k_x k_y + 2[\nu_{xy}(\zeta J_2^x + \Lambda^2 J_0^y) + \nu_y\Lambda(\zeta J_1^x + J_1^y)]k_y^2\}\delta l, \tag{A23}$$

$$\Sigma_{yy}(\mathbf{k},0) = -\frac{\lambda_y^2 D\Lambda}{8\pi^2}\{[\nu_x(\zeta J_2^x + \Lambda^2 J_0^y) + 4\nu_{xy}\Lambda(\zeta J_1^x + J_1^y) + 3\nu_y(\zeta\Lambda^2 J_0^x + J_2^y)]k_y^2 + 2[\nu_{xy}(\zeta\Lambda^2 J_0^x + J_2^y) + \nu_x\Lambda(\zeta J_1^x + J_1^y)]k_x k_y\}\delta l. \tag{A24}$$

Using the definitions of the couplings $g, f_\nu, r_\nu, r_\lambda$ provided in Eq. (50) of the main text and performing a change of variables, the integrals in Eqs. (A19) and (A20) can be expressed as

$$J_i^x = \frac{1}{\nu_x^3\Lambda^2} J_i(1,r_\nu), \tag{A25}$$

$$J_i^y = \frac{1}{\nu_x^3 \Lambda^2} J_i(r_\nu, 1), \tag{A26}$$

where

$$J_i(a,b) = \int_{-1}^{+1} \frac{s^i\, ds}{(as^2 + 2f_\nu s + b)^3}. \tag{A27}$$

After some algebra, we can make these integrals explicit in term of the couplings,

$$\begin{aligned}
J_0(a,b) = {} & \frac{1}{8\left(ab - f_\nu^2\right)^2}\left\{(a+f_\nu)\frac{2\left(ab-f_\nu^2\right)+3a(a+2f_\nu+b)}{(a+2f_\nu+b)^2} + (a-f_\nu)\frac{2\left(ab-f_\nu^2\right)+3a(a-2f_\nu+b)}{(a-2f_\nu+b)^2}\right. \\
& \left. + \frac{3a^2}{\sqrt{ab-f_\nu^2}}\left[\tan^{-1}\left(\frac{a+f_\nu}{\sqrt{ab-f_\nu^2}}\right) + \tan^{-1}\left(\frac{a-f_\nu}{\sqrt{ab-f_\nu^2}}\right)\right]\right\}, \\
J_1(a,b) = {} & -\frac{1}{8\left(ab - f_\nu^2\right)^2}\left\{\frac{2\left(ab-f_\nu^2\right)(f_\nu+b)}{(a+2f_\nu+b)^2} + \frac{3f_\nu(a+f_\nu)}{a+2f_\nu+b} + \frac{2\left(ab-f_\nu^2\right)(f_\nu-b)}{(a-2f_\nu+b)^2} + \frac{3f_\nu(a-f_\nu)}{a-2f_\nu+b}\right. \\
& \left. + \frac{3af_\nu}{\sqrt{ab-f_\nu^2}}\left[\tan^{-1}\left(\frac{a+f_\nu}{\sqrt{ab-f_\nu^2}}\right) + \tan^{-1}\left(\frac{a-f_\nu}{\sqrt{ab-f_\nu^2}}\right)\right]\right\}, \\
J_2(a,b) = {} & \frac{1}{8\left(ab - f_\nu^2\right)^2}\left\{\frac{2(a-b)\left[ab(a+b)^2 + 2(a^2+4ab+b^2)f_\nu^2 - 16f_\nu^4\right]}{\left[(a+b)^2 - 4f_\nu^2\right]^2}\right. \\
& \left. + \frac{2f_\nu^2+ab}{\sqrt{ab-f_\nu^2}}\left[\tan^{-1}\left(\frac{a+f_\nu}{\sqrt{ab-f_\nu^2}}\right) + \tan^{-1}\left(\frac{a-f_\nu}{\sqrt{ab-f_\nu^2}}\right)\right]\right\}.
\end{aligned}$$

It is now convenient to write the contributions to the coarse-grained propagator by gathering together the various terms, according to which parameter they renormalize in the original gHK equation,

$$\begin{aligned}
\Sigma &= \Sigma_{xx} + \Sigma_{xy} + \Sigma_{yx} + \Sigma_{yy} \\
&\approx \left(\Sigma_{\nu_x}\nu_x k_x^2 + 2\Sigma_{\nu_{xy}}\nu_{xy}k_xk_y + \Sigma_{\nu_y}\nu_y k_y^2\right)\delta l.
\end{aligned} \tag{A28}$$

Using Eq. (50) of the main text, the functions on the right-hand side of Eq. (A28) read

$$\begin{aligned}
\Sigma_{\nu_x} = {} & -2g\{3[\zeta J_2(1,r_\nu) + J_0(r_\nu,1)] \\
& + 2(r_\nu + 2f_\nu)[\zeta J_1(1,r_\nu) + J_1(r_\nu,1)] \\
& + (r_\nu + 2f_\nu r_\lambda)[\zeta J_0(1,r_\nu) + J_2(r_\nu,1)]\},
\end{aligned} \tag{A29}$$

$$\begin{aligned}
\Sigma_{\nu_{xy}} = {} & -\frac{g}{f_\nu}\{2(f_\nu + 2r_\lambda)[\zeta J_2(1,r_\nu) + J_0(r_\nu,1)] \\
& + \left(2r_\nu + 8r_\lambda f_\nu + r_\lambda^2\right)[\zeta J_1(1,r_\nu) + J_1(r_\nu,1)] \\
& + r_\lambda(4r_\nu + r_\lambda f_\nu)[\zeta J_0(1,r_\nu) + J_2(r_\nu,1)]\},
\end{aligned} \tag{A30}$$

$$\begin{aligned}
\Sigma_{\nu_y} = {} & -2\frac{gr_\lambda}{r_\nu}\{(r_\lambda + 2f_\nu)[\zeta J_2(1,r_\nu) + J_0(r_\nu,1)] \\
& + 2(r_\nu + 2f_\nu r_\lambda)[\zeta J_1(1,r_\nu) + J_1(r_\nu,1)] \\
& + 3r_\lambda r_\nu[\zeta J_0(1,r_\nu) + J_2(r_\nu,1)]\},
\end{aligned} \tag{A31}$$

so that the coarse-grained propagator can be finally written as

$$\begin{aligned}
G_0^<(\mathbf{k},\omega) = {} & \left[\nu_x\left(1 - \Sigma_{\nu_x}\delta l\right)k_x^2 + 2\nu_{xy}\left(1 - \Sigma_{\nu_{xy}}\delta l\right)k_xk_y \right. \\
& \left. + \nu_y\left(1 - \Sigma_{\nu_y}\delta l\right)k_y^2 - i\omega\right]^{-1}.
\end{aligned} \tag{A32}$$

Hence, the coarse-grained surface tension parameters are $\nu_x^< = \nu_x(1 - \Sigma_{\nu_x}\delta l)$, $\nu_{xy}^< = \nu_{xy}(1 - \Sigma_{\nu_{xy}}\delta l)$, and $\nu_y^< = \nu_y(1 - \Sigma_{\nu_y}\delta l)$. After rescaling as in Eq. (25), the corresponding flow equations become Eqs. (44)–(46) of the main text.

The renormalization of the noise variance is calculated from the standard diagram shown in Fig. 13. Due to the existence of two different vertices, four different contributions occur, analogously to the renormalization of the propagator. In the symmetric momentum variable $\mathbf{j}$ they read, to leading order,

$$\begin{aligned}
\Phi_{lm}(\mathbf{k},\omega) = {} & \lambda_l\lambda_m D^2 k_l k_m \int^> \frac{d\mathbf{j}}{(2\pi)^2}\int\frac{d\Omega}{2\pi} \\
& \times \left|G_0\left(\frac{\hat{k}}{2} + \hat{j}\right)\right|^2\left|G_0\left(\frac{\hat{k}}{2} - \hat{j}\right)\right|^2.
\end{aligned} \tag{A33}$$

Since all contributions given by Eq. (A33) are proportional to $k_l k_m$, they can be neglected in the limit $k_{x,y} \to 0$. Hence,

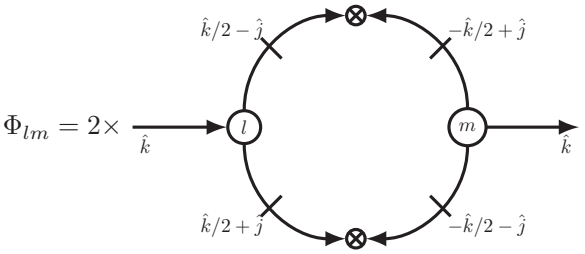

FIG. 13. Generic diagrammatic representation of the four different contributions Φ_{xx}, Φ_{xy}, Φ_{yx}, and Φ_{yy} to the renormalization of the noise variance $2D$ for the gHK and the aKPZ equations. For each equation the exact meaning of the solid lines differ; see Eq. (A33) for the former and Eq. (B18) for the latter.

the coefficient D is not renormalized to all orders of the perturbation series, and its flow equation is simply given by Eq. (49) of the main text. Finally, the one-loop contributions to the renormalization of the nonlinearities $\lambda_{x,y}$ cancel out [47], giving rise to Eqs. (47) and (48) of the main text, thus completing the DRG flow for the gHK equation.

1. Standard HK equation

The RG flow for the standard HK equation is retrieved from the one derived for the gHK equation by setting $f_\nu = 0$ and $r_\lambda = 0$. In this case the J_i integrals [Eq. (A27)] reduce to

$$J_0(a,b) = \frac{1}{8b^2}\left[\frac{6a+10b}{(a+b)^2} + \frac{6}{\sqrt{ab}}\tan^{-1}\left(\sqrt{\frac{a}{b}}\right)\right], \quad \text{(A34)}$$

$$J_2(a,b) = \frac{1}{8ab}\left[\frac{2(a-b)}{(a+b)^2} + \frac{2}{\sqrt{ab}}\tan^{-1}\left(\sqrt{\frac{a}{b}}\right)\right], \quad \text{(A35)}$$

whereas J_1 is identically equal to zero. The condition $r_\lambda = 0$ implies $\lambda_y = 0$, so that $\Sigma_{xy} = \Sigma_{yx} = \Sigma_{yy} = 0$. The condition $f_\nu = 0$ implies $\nu_{xy} = 0$, so that in this case Σ_{xx} does not generate ν_{xy} under coarse graining, provided its bare value is zero.

2. gHK equation for $\zeta = 1$

If $\zeta = 1$, the functions intervening in the RG flow of the gHK equation simplify somewhat. Thus,

$$\begin{aligned}
J_2(1,r_\nu) + J_0(r_\nu,1) = \frac{1}{8\left(r_\nu - f_\nu^2\right)^2}\Bigg\{&\frac{4f_\nu^2(5r_\nu-1) - 2r_\nu\left(1+4r_\nu+3r_\nu^2\right)}{4f_\nu^2-(1+r_\nu)^2} \\
&+ \frac{3r_\nu^2}{\sqrt{r_\nu - f_\nu^2}}\left[\tan^{-1}\left(\frac{r_\nu+f_\nu}{\sqrt{r_\nu-f_\nu^2}}\right) + \tan^{-1}\left(\frac{r_\nu-f_\nu}{\sqrt{r_\nu-f_\nu^2}}\right)\right] \\
&+ \frac{2f_\nu^2+r_\nu}{\sqrt{r_\nu - f_\nu^2}}\left[\tan^{-1}\left(\frac{1+f_\nu}{\sqrt{r_\nu-f_\nu^2}}\right) + \tan^{-1}\left(\frac{1-f_\nu}{\sqrt{r_\nu-f_\nu^2}}\right)\right]\Bigg\}, \\
J_1(1,r_\nu) + J_1(r_\nu,1) = \frac{1}{8\left(r_\nu - f_\nu^2\right)^2}\Bigg\{&\frac{2f_\nu\left(3-8f_\nu^2+2r_\nu+3r_\nu^2\right)}{4f_\nu^2-(1+r_\nu)^2} \\
&- \frac{3f_\nu r_\nu}{\sqrt{r_\nu - f_\nu^2}}\left[\tan^{-1}\left(\frac{r_\nu+f_\nu}{\sqrt{r_\nu-f_\nu^2}}\right) + \tan^{-1}\left(\frac{r_\nu-f_\nu}{\sqrt{r_\nu-f_\nu^2}}\right)\right] \\
&- \frac{3f_\nu}{\sqrt{r_\nu - f_\nu^2}}\left[\tan^{-1}\left(\frac{1+f_\nu}{\sqrt{r_\nu-f_\nu^2}}\right) + \tan^{-1}\left(\frac{1-f_\nu}{\sqrt{r_\nu-f_\nu^2}}\right)\right]\Bigg\}, \\
J_0(1,r_\nu) + J_2(r_\nu,1) = \frac{1}{8\left(r_\nu - f_\nu^2\right)^2}\Bigg\{&\frac{4f_\nu^2(5-r_\nu) - 2r_\nu(4+r_\nu) - 6}{4f_\nu^2-(1+r_\nu)^2} \\
&+ \frac{2f_\nu^2+r_\nu}{\sqrt{r_\nu - f_\nu^2}}\left[\tan^{-1}\left(\frac{r_\nu+f_\nu}{\sqrt{r_\nu-f_\nu^2}}\right) + \tan^{-1}\left(\frac{r_\nu-f_\nu}{\sqrt{r_\nu-f_\nu^2}}\right)\right] \\
&+ \frac{3}{\sqrt{r_\nu - f_\nu^2}}\left[\tan^{-1}\left(\frac{1+f_\nu}{\sqrt{r_\nu-f_\nu^2}}\right) + \tan^{-1}\left(\frac{1-f_\nu}{\sqrt{r_\nu-f_\nu^2}}\right)\right]\Bigg\}.
\end{aligned}$$

These formulas can be employed in order to rewrite the flow of the couplings, which reads

$$\begin{aligned}
\frac{dr_\nu}{dl} = &-\frac{g}{\left(r_\nu - f_\nu^2\right)^2}\Bigg\{\frac{p_{r1}(r_\lambda)}{4f_\nu^2-(1+r_\nu)^2} + \frac{p_{r2}(r_\lambda)}{4\sqrt{r_\nu-f_\nu^2}}\left[\tan^{-1}\left(\frac{1+f_\nu}{\sqrt{r_\nu-f_\nu^2}}\right) + \tan^{-1}\left(\frac{1-f_\nu}{\sqrt{r_\nu-f_\nu^2}}\right)\right] \\
&+ \frac{p_{r3}(r_\lambda)}{4\sqrt{r_\nu-f_\nu^2}}\left[\tan^{-1}\left(\frac{r_\nu+f_\nu}{\sqrt{r_\nu-f_\nu^2}}\right) + \tan^{-1}\left(\frac{r_\nu-f_\nu}{\sqrt{r_\nu-f_\nu^2}}\right)\right]\Bigg\}, \quad \text{(A36)} \\
\frac{df_\nu}{dl} = &\frac{g}{2\left(r_\nu - f_\nu^2\right)^2}\Bigg\{\frac{p_{f1}(r_\lambda)}{4f_\nu^2-(1+r_\nu)^2} - \frac{p_{f2}(r_\lambda)}{4\sqrt{r_\nu-f_\nu^2}}\left[\tan^{-1}\left(\frac{1+f_\nu}{\sqrt{r_\nu-f_\nu^2}}\right) + \tan^{-1}\left(\frac{1-f_\nu}{\sqrt{r_\nu-f_\nu^2}}\right)\right] \\
&- \frac{p_{f3}(r_\lambda)}{4\sqrt{r_\nu-f_\nu^2}}\left[\tan^{-1}\left(\frac{r_\nu+f_\nu}{\sqrt{r_\nu-f_\nu^2}}\right) + \tan^{-1}\left(\frac{r_\nu-f_\nu}{\sqrt{r_\nu-f_\nu^2}}\right)\right]\Bigg\}, \quad \text{(A37)} \\
\frac{dg}{dl} = 2g + &\frac{3g^2}{\left(r_\nu - f_\nu^2\right)^2}\Bigg\{\frac{p_{g1}}{4f_\nu^2-(1+r_\nu)^2} - \frac{p_{g2}(r_\lambda)}{4\sqrt{r_\nu-f_\nu^2}}\left[\tan^{-1}\left(\frac{1+f_\nu}{\sqrt{r_\nu-f_\nu^2}}\right) + \tan^{-1}\left(\frac{1-f_\nu}{\sqrt{r_\nu-f_\nu^2}}\right)\right] \\
&- \frac{p_{g3}(r_\lambda)}{4\sqrt{r_\nu-f_\nu^2}}\left[\tan^{-1}\left(\frac{r_\nu+f_\nu}{\sqrt{r_\nu-f_\nu^2}}\right) + \tan^{-1}\left(\frac{r_\nu-f_\nu}{\sqrt{r_\nu-f_\nu^2}}\right)\right]\Bigg\}, \quad \text{(A38)}
\end{aligned}$$

with

$$p_{r1}(r_\lambda) = \left(f_\nu^2 - r_\nu\right)\left[16f_\nu^2 - (r_\nu+1)(3r_\nu+5)\right]r_\lambda^2 - f_\nu\left[2f_\nu^2\left(r_\nu^2 - 4r_\nu - 1\right) + r_\nu^3 + 2r_\nu^2 + 5r_\nu\right]r_\lambda$$
$$- r_\nu\left[16f_\nu^4 + 8r_\nu f_\nu^3 - \left(5r_\nu^2 + 24r_\nu + 3\right)f_\nu^2 - \left(3r_\nu^3 + 2r_\nu^2 + 3r_\nu\right)f_\nu + 5r_\nu^3 + 8r_\nu^2 + 3r_\nu\right],$$

$$p_{r2}(r_\lambda) = 10\left(f_\nu^2 - r_\nu\right)r_\lambda^2 + 2f_\nu\left(5r_\nu - 2f_\nu^2\right)r_\lambda + 6r_\nu\left(r_\nu - f_\nu r_\nu - f_\nu^2\right),$$

$$p_{r3}(r_\lambda) = 6r_\nu\left(f_\nu^2 - r_\nu\right)r_\lambda^2 + 2f_\nu r_\nu\left(r_\nu + 2f_\nu^2\right)r_\lambda + 2r_\nu^2\left(5r_\nu - 3f_\nu r_\nu - 5f_\nu^2\right),$$

$$p_{f1}(r_\lambda) = f_\nu\left(f_\nu^2 - r_\nu\right)(1 - r_\nu)r_\lambda^2 + \left[f_\nu^4(4r_\nu - 52) + f_\nu^2\left(10r_\nu^2 + 56r_\nu + 14\right) - 8r_\nu\left(r_\nu^2 + 2r_\nu + 1\right)\right]r_\lambda$$
$$+ 2f_\nu\left[8f_\nu^3(r_\nu + 2f_\nu) - f_\nu^2\left(5r_\nu^2 + 23r_\nu + 4\right) - f_\nu r_\nu\left(3r_\nu^2 + 2r_\nu + 3\right) + r_\nu\left(5r_\nu^2 + 7r_\nu + 4\right)\right],$$

$$p_{f2}(r_\lambda) = 4\left(7f_\nu^2 - 4r_\nu\right)r_\lambda + 4f_\nu\left(4r_\nu - 3f_\nu r_\nu - 4f_\nu^2\right),$$

$$p_{f3}(r_\lambda) = 2f_\nu\left(r_\nu - f_\nu^2\right)r_\lambda^2 + 4\left(-4r_\nu^2 + 5f_\nu^2 r_\nu + 2f_\nu^4\right)r_\lambda + 4f_\nu r_\nu\left(5r_\nu - 3f_\nu r_\nu - 5f_\nu^2\right),$$

$$p_{g1}(r_\lambda) = r_\lambda\left[2f_\nu^3(r_\nu - 5) + f_\nu\left(r_\nu^2 + 4r_\nu + 3\right)\right] + 8f_\nu^3(r_\nu + 2f_\nu) - f_\nu^2\left(5r_\nu^2 + 24r_\nu + 3\right)$$
$$- f_\nu r_\nu\left(3r_\nu^2 + 2r_\nu + 3\right) + r_\nu\left(5r_\nu^2 + 8r_\nu + 3\right),$$

$$p_{g2}(r_\lambda) = 6f_\nu r_\lambda + 6\left(r_\nu - f_\nu r_\nu - f_\nu^2\right), \quad p_{g3}(r_\lambda) = 2f_\nu\left(2f_\nu^2 + r_\nu\right)r_\lambda + 2r_\nu\left(5r_\nu - 3f_\nu r_\nu - 5f_\nu^2\right).$$

APPENDIX B: DYNAMIC RENORMALIZATION GROUP ANALYSIS OF THE ANISOTROPIC KARDAR-PARISI-ZHANG EQUATION

For the aKPZ equation, the diagrammatic expansion of the integrals that contribute to the renormalization of the bare propagator can be also sketched using general notation as shown in Fig. 12. Again $l,m = x,y$ in all possible combinations, leading to four different contributions, which will be denoted Σ_{xx}, Σ_{xy}, Σ_{yx}, and Σ_{yy}, as in the gHK case. Naturally, the values of these differ for each equation; we hope the context will hinder any potential ambiguity, as we are providing separate discussions for the two equations. After the usual symmetrization of the integration variables $(\mathbf{q},\Omega) \to (\mathbf{j} + \mathbf{k}/2, \Omega + \omega/2)$, these contributions read

$$\Sigma_{lm}(\mathbf{k},\omega) = 2\lambda_l\lambda_m D \int^> \frac{d\mathbf{j}}{(2\pi)^2}\int\frac{d\Omega}{2\pi}\left(j_l^2 - \frac{k_l^2}{4}\right)\left(\frac{k_m}{2} + j_m\right)k_m \times \left|G_0\left(\frac{\hat{k}}{2} + \hat{j}\right)\right|^2 G_0\left(\frac{\hat{k}}{2} - \hat{j}\right), \tag{B1}$$

where again $G_0(\hat{k})$ is shorthand notation for the bare propagator, which now reads

$$G_0(\hat{k}) = \left[\nu_x k_x^2 + \nu_y k_y^2 - i\omega\right]^{-1}. \tag{B2}$$

An expansion to first order in $k_x/j_x, k_y/j_y \ll 1$ leads to

$$\lim_{\omega\to 0}|G_0(\hat{k}/2 + \hat{j})|^2 \sim \frac{1}{\Delta^2 + \Omega^2}\left[1 - \frac{2\Delta}{\Delta^2 + \Omega^2}(\nu_x j_x k_x + \nu_y j_y k_y)\right], \tag{B3}$$

$$\lim_{\omega\to 0} G_0(\hat{k}/2 - \hat{j}) \sim \frac{1}{\Delta + i\Omega}\left[1 + \frac{1}{\Delta + i\Omega}(\nu_x j_x k_x + \nu_y j_y k_y)\right], \tag{B4}$$

where $\Delta = \nu_x j_x^2 + \nu_y j_y^2$. Using these results in Eq. (B1) and after integration over the frequency variable Ω, to second order in the components of $\mathbf{k}$ we get

$$\Sigma_{lm}(\mathbf{k},0) = \frac{\lambda_l\lambda_m D}{16\pi^2}\int^> \frac{d\mathbf{j}}{\Delta^2}\Big[\, j_l^2 k_m^2 - \frac{2}{\Delta}k_m j_l^2 j_m \times (\nu_x k_x j_x + \nu_y k_y j_y)\Big]. \tag{B5}$$

Considering all possible combinations for $l,m = x,y$, we obtain the coarse-grained propagator, $\Sigma = \Sigma_{xx} + \Sigma_{xy} + \Sigma_{yx} + \Sigma_{yy}$. We now take into account that the momentum shell is symmetric with respect to j_x and j_y; hence, contributions from odd functions cancel out in these integrals, leading to

$$\Sigma_{xx}(\mathbf{k},0) = \frac{\lambda_x^2 D}{16\pi^2}\int^> \frac{d\mathbf{j}}{\Delta^2}\left(j_x^2 - \frac{2}{\Delta}\nu_x j_x^4\right)k_x^2, \tag{B6}$$

$$\Sigma_{xy}(\mathbf{k},0) = \frac{\lambda_x\lambda_y D}{16\pi^2}\int^> \frac{d\mathbf{j}}{\Delta^2}\left(j_x^2 - \frac{2}{\Delta}\nu_y j_x^2 j_y^2\right)k_y^2, \tag{B7}$$

$$\Sigma_{yx}(\mathbf{k},0) = \frac{\lambda_x\lambda_y D}{16\pi^2}\int^> \frac{d\mathbf{j}}{\Delta^2}\left(j_y^2 - \frac{2}{\Delta}\nu_x j_x^2 j_y^2\right)k_x^2, \tag{B8}$$

$$\Sigma_{yy}(\mathbf{k},0) = \frac{\lambda_y^2 D}{16\pi^2}\int^> \frac{d\mathbf{j}}{\Delta^2}\left(j_y^2 - \frac{2}{\Delta}\nu_y j_y^4\right)k_y^2. \tag{B9}$$

As in the gHK case, the next step is to calculate the contributions to these integrals induced by the **k** dependence of the integration limits defining the momentum shell. Now we can split the momentum integrals in only two parts,

$$\int^{>}\frac{d\mathbf{j}}{4\Delta^2}\left(j_x^2-\frac{2}{\Delta}\nu_x j_x^4\right)=\int_{\Lambda/b}^{\Lambda}dj_x\int_0^{\Lambda}dj_y\left(\frac{j_x^2}{\Delta^2}-2\nu_x\frac{j_x^4}{\Delta^3}\right)+\int_{\Lambda/b^\zeta}^{\Lambda}dj_y\int_0^{\Lambda}dj_x\left(\frac{j_x^2}{\Delta^2}-2\nu_x\frac{j_x^4}{\Delta^3}\right)$$
$$=\int_{\Lambda/b}^{\Lambda}dj_x\,j_x^2\left(I_{02}^y-2\nu_x j_x^2 I_{03}^y\right)+\int_{\Lambda/b^\zeta}^{\Lambda}dj_y\left(I_{22}^x-2\nu_x I_{43}^x\right),\tag{B10}$$

$$\int^{>}\frac{d\mathbf{j}}{4\Delta^2}\left(j_x^2-\frac{2}{\Delta}\nu_y j_x^2 j_y^2\right)=\int_{\Lambda/b}^{\Lambda}dj_x\,j_x^2\left(I_{02}^y-2\nu_y I_{23}^y\right)+\int_{\Lambda/b^\zeta}^{\Lambda}dj_y\left(I_{22}^x-2\nu_y j_y^2 I_{23}^x\right),\tag{B11}$$

$$\int^{>}\frac{d\mathbf{j}}{4\Delta^2}\left(j_y^2-\frac{2}{\Delta}\nu_x j_x^2 j_y^2\right)=\int_{\Lambda/b}^{\Lambda}dj_x\left(I_{22}^y-2\nu_x j_x^2 I_{23}^y\right)+\int_{\Lambda/b^\zeta}^{\Lambda}dj_y\,j_y^2\left(I_{02}^x-2\nu_x I_{23}^x\right),\tag{B12}$$

$$\int^{>}\frac{d\mathbf{j}}{4\Delta^2}\left(j_y^2-\frac{2}{\Delta}\nu_y j_y^4\right)=\int_{\Lambda/b}^{\Lambda}dj_x\left(I_{22}^y-2\nu_y I_{43}^y\right)+\int_{\Lambda/b^\zeta}^{\Lambda}dj_y\,j_y^2\left(I_{02}^x-2\nu_y j_y^2 I_{03}^x\right),\tag{B13}$$

where the values of the integrals

$$I_{ij}^x=\int_0^{\Lambda}ds\,s^i\left(\nu_x s^2+\nu_y j_y^2\right)^{-j},\tag{B14}$$

$$I_{ij}^y=\int_0^{\Lambda}ds\,s^i\left(\nu_x j_x^2+\nu_y s^2\right)^{-j},\tag{B15}$$

are provided in Table I. The remaining integrals are solved perturbatively for $\delta l\to 0$, using that $\Lambda/b=\Lambda e^{-\delta l}\sim\Lambda(1-\delta l)$ and $\Lambda/b^\zeta\sim\Lambda(1-\zeta\delta l)$. We thus get

$$\Sigma_{xx}(\mathbf{k},0)=\frac{\lambda_x^2 D}{16\pi^2\nu_x}(\zeta-1)\left[\frac{3\nu_x+\nu_y}{(\nu_x+\nu_y)^2}-B_{\nu_x,\nu_y,\zeta}\right]k_x^2\delta l,$$
$$\Sigma_{xy}(\mathbf{k},0)=\frac{\lambda_x\lambda_y D}{16\pi^2\nu_x}(\zeta-1)\left[B_{\nu_x,\nu_y,\zeta}-\frac{3\nu_x+\nu_y}{(\nu_x+\nu_y)^2}\right]k_y^2\delta l,$$
$$\Sigma_{yx}(\mathbf{k},0)=\frac{\lambda_x\lambda_y D}{16\pi^2\nu_y}(\zeta-1)\left[B_{\nu_x,\nu_y,\zeta}+\frac{\nu_x+3\nu_y}{(\nu_x+\nu_y)^2}\right]k_x^2\delta l,$$
$$\Sigma_{yy}(\mathbf{k},0)=\frac{\lambda_y^2 D}{16\pi^2\nu_y}(1-\zeta)\left[\frac{\nu_x+3\nu_y}{(\nu_x+\nu_y)^2}+B_{\nu_x,\nu_y,\zeta}\right]k_y^2\delta l,$$

TABLE I. Definite integrals $I_{ij}=I_{ij}^x$ [Eq. (B14)] for $a=\nu_y j_y^2$ and $b=\nu_x$, and $I_{ij}=I_{ij}^y$ [Eq. (B15)] for $a=\nu_x j_x^2$ and $b=\nu_y$.

I_{02}	$\frac{1}{2a}\left[\frac{\tan^{-1}(\Lambda\sqrt{b/a})}{\sqrt{ab}}+\frac{\Lambda}{a+b\Lambda^2}\right]$
I_{22}	$\frac{1}{2b}\left[\frac{\tan^{-1}(\Lambda\sqrt{b/a})}{\sqrt{ab}}-\frac{\Lambda}{a+b\Lambda^2}\right]$
I_{03}	$\frac{1}{8a^2}\left[\frac{3\tan^{-1}(\Lambda\sqrt{b/a})}{\sqrt{ab}}+\frac{\Lambda(5a+3b\Lambda^2)}{(a+b\Lambda^2)^2}\right]$
I_{23}	$\frac{1}{8ab}\left[\frac{3\tan^{-1}(\Lambda\sqrt{b/a})}{\sqrt{ab}}+\frac{\Lambda(b\Lambda^2-a)}{(a+b\Lambda^2)^2}\right]$
I_{43}	$\frac{1}{8b^2}\left[\frac{3\tan^{-1}(\Lambda\sqrt{b/a})}{\sqrt{ab}}-\frac{\Lambda(3a+5b\Lambda^2)}{(a+b\Lambda^2)^2}\right]$

where

$$B_{\nu_x,\nu_y,\zeta}=\frac{\tan^{-1}(\sqrt{\nu_y/\nu_x})+\zeta\tan^{-1}(\sqrt{\nu_x/\nu_y})}{(\zeta-1)(\nu_x\nu_y)^{1/2}}.\tag{B16}$$

At this stage of the calculation it is convenient to gather the factors together, according to the parameter in the original aKPZ equation which they renormalize. We thus introduce functions $\Sigma_{\nu_{x,y}}$ through $\Sigma_{\nu_x}\delta l\,\nu_x k_x^2\equiv\Sigma_{xx}(\mathbf{k},0)+\Sigma_{yx}(\mathbf{k},0)$ and $\Sigma_{\nu_y}\delta l\,\nu_y k_y^2\equiv\Sigma_{xy}(\mathbf{k},0)+\Sigma_{yy}(\mathbf{k},0)$, so that the coarse-grained propagator reads

$$G_0^<(\mathbf{k},\omega)=\left[\nu_x\left(1-\Sigma_{\nu_x}\delta l\right)k_x^2+\nu_y\left(1-\Sigma_{\nu_y}\delta l\right)k_y^2-i\omega\right]^{-1}.\tag{B17}$$

Hence, the coarse-grained surface tension parameters are $\nu_x^<=\nu_x(1-\Sigma_{\nu_x}\delta l)$ and $\nu_y^<=\nu_y(1-\Sigma_{\nu_y}\delta l)$. After rescaling as in Eq. (25), the corresponding flow equations become Eqs. (61) and (62) of the main text.

The renormalization of the noise variance is again calculated from the standard diagram in Fig. 13. Similar considerations apply as in the case of the gHK equation. However, now noise does renormalize nontrivially. Indeed, in the symmetric momentum variable **j**, the contributions to the coarse-grained noise variance read

$$\Phi_{lm}(\mathbf{k},\omega)$$
$$=\lambda_l\lambda_m D^2\int^{>}\frac{d\mathbf{j}}{(2\pi)^2}\int\frac{d\Omega}{2\pi}\left(\frac{k_l^2}{4}-j_l^2\right)\left(\frac{k_m^2}{4}-j_m^2\right)$$
$$\times\left|G_0\left(\frac{\hat{k}}{2}+\hat{j}\right)\right|^2\left|G_0\left(\frac{\hat{k}}{2}-\hat{j}\right)\right|^2,\tag{B18}$$

where $l,m=x,y$ in all four possible combinations. Taking into account that in the perturbative expansion of Φ_{lm} we only have to retain the zeroth-order contribution in **k** components and that

$$\lim_{\omega\to 0}|G_0(\hat{k}/2-\hat{j})|^2\sim\frac{1}{\Delta^2+\Omega^2},\tag{B19}$$

after the integration in the frequency variable Ω, we obtain

$$\Phi_{lm}(\mathbf{k},0) \sim \frac{\lambda_l \lambda_m D^2}{16\pi^2} \int^{>} d\mathbf{j}\, \frac{j_l^2 j_m^2}{\Delta^3}. \tag{B20}$$

The four contributions are calculated as

$$\Phi_{xx}(\mathbf{k},0) = \frac{\lambda_x^2 D^2}{16\pi^2} \int^{>} d\mathbf{j}\, \frac{j_x^4}{\Delta^3} = \frac{\lambda_x^2 D^2}{4\pi^2}\left[\int_{\Lambda/b}^{\Lambda} dj_x\, j_x^4 I_{03}^{y} + \int_{\Lambda/b^\zeta}^{\Lambda} dj_y\, I_{43}^{x}\right]$$
$$\sim \frac{\lambda_x^2 D^2}{32\pi^2 \nu_x^2}(\zeta-1)\left[3B_{\nu_x,\nu_y,\zeta} - \frac{5\nu_x+3\nu_y}{(\nu_x+\nu_y)^2}\right]\delta l, \tag{B21}$$

$$\Phi_{xy}(\mathbf{k},0) = \Phi_{yx}(\mathbf{k},0) = \frac{\lambda_x \lambda_y D^2}{16\pi^2} \int^{>} d\mathbf{j}\, \frac{j_x^2 j_y^2}{\Delta^3} = \frac{\lambda_x \lambda_y D^2}{4\pi^2}\left[\int_{\Lambda/b}^{\Lambda} dj_x\, j_x^2 I_{23}^{y} + \int_{\Lambda/b^\zeta}^{\Lambda} dj_y\, j_y^2 I_{23}^{x}\right]$$
$$\sim \frac{\lambda_x \lambda_y D^2}{32\pi^2 \nu_x \nu_y}(\zeta-1)\left[B_{\nu_x,\nu_y,\zeta} + \frac{\nu_x-\nu_y}{(\nu_x+\nu_y)^2}\right]\delta l, \tag{B22}$$

$$\Phi_{yy}(\mathbf{k},0) = \frac{\lambda_y^2 D^2}{16\pi^2} \int^{>} d\mathbf{j}\, \frac{j_y^4}{\Delta^3} = \frac{\lambda_y^2 D^2}{4\pi^2}\left[\int_{\Lambda/b}^{\Lambda} dj_x\, I_{43}^{y} + \int_{\Lambda/b^\zeta}^{\Lambda} dj_y\, j_y^4 I_{03}^{x}\right]$$
$$\sim \frac{\lambda_y^2 D^2}{32\pi^2 \nu_y^2}(\zeta-1)\left[3B_{\nu_x,\nu_y,\zeta} + \frac{3\nu_x+5\nu_y}{(\nu_x+\nu_y)^2}\right]\delta l, \tag{B23}$$

and finally

$$\Phi(\mathbf{k},0) = \sum_{l,m=x,y} \Phi_{lm}(\mathbf{k},0)$$
$$= \frac{D^2}{32\pi^2}(\zeta-1)\left\{3B_{\nu_x,\nu_y,\zeta}\left(\frac{\lambda_x^2}{\nu_x^2} + \frac{2\lambda_x\lambda_y}{3\nu_x\nu_y} + \frac{\lambda_y^2}{\nu_y^2}\right) + \left[\frac{\lambda_y^2(3\nu_x+5\nu_y)}{\nu_y^2(\nu_x+\nu_y)^2} + \frac{2\lambda_x\lambda_y(\nu_x-\nu_y)}{\nu_x\nu_y(\nu_x+\nu_y)^2} - \frac{\lambda_x^2(5\nu_x+3\nu_y)}{\nu_x^2(\nu_x+\nu_y)^2}\right]\right\}\delta l. \tag{B24}$$

Note this function is $\mathbf{k}$ independent; hence, it implies a nontrivial effect of coarse graining in the noise variance for the aKPZ equation. By introducing a function Φ_D through $\Phi_D D\delta l \equiv \Phi(\mathbf{k},0)$, the coarse-grained noise variance is $D^< = D(1+\Phi_D\delta l)$. After rescaling as in Eq. (25), the corresponding flow equation becomes Eq. (65) of the main text. Finally, the one-loop contributions to the renormalization of the nonlinearities $\lambda_{x,y}$ cancel out [47], giving rise to Eqs. (63) and (64) of the main text, thus completing the DRG flow for the aKPZ equation.

[1] C. Misbah, O. Pierre-Louis, and Y. Saito, Rev. Mod. Phys. **82**, 981 (2010).
[2] M. J. Alava, P. K. V. V. Nukala, and S. Zapperi, Adv. Phys. **55**, 349 (2006).
[3] D. Bonamy and E. Bouchaud, Phys. Rep. **498**, 1 (2011).
[4] R. Pastor-Satorras and D. H. Rothman, J. Stat. Phys. **93**, 477 (1998).
[5] I. Rodríguez-Irturbe and A. Rinaldo, *Fractal River Basins: Chance and Self-Organization* (Cambridge University Press, Cambridge, UK, 2001).
[6] A.-L. Barabási and H. E. Stanley, *Fractal Concepts in Surface Growth* (Cambridge University Press, Cambridge, UK, 1995).
[7] M. Henkel and M. Pleimling, *Non-Equilibrium Phase Transitions: Ageing and Dynamical Scaling Far from Equilibrium* (Springer, Dordrecht, 2010), Vol. 2.
[8] U. C. Täuber, Critical Dynamics: A Field Theory Approach to Equilibrium and Non-equilibrium Scaling Behavior (unpublished); http://www.phys.vt.edu/~tauber
[9] G. Grinstein, D.-H. Lee, and S. Sachdev, Phys. Rev. Lett. **64**, 1927 (1990).
[10] G. Grinstein, J. Appl. Phys. **69**, 5441 (1991).
[11] G. Grinstein, *Scale Invariance, Interfaces, and Non-equilibrium Dynamics*, edited by A. J. McKane, M. Droz, J. Vannimenus, and D. Wolf (Plenum Press, New York, 1995).
[12] B. Schmittmann and R. K. P. Zia, in *Phase Transitions and Critical Phenomenas*, edited by C. Domb and J. L. Lebowitz (Academic Press, London, 2000), Vol. 17.
[13] K. Christensen and N. R. Moloney, *Complexity and Criticalitys* (Imperial College Press, London, 2005).
[14] M. Kardar, *Statistical Physics of Fields* (Cambridge University Press, Cambridge, UK, 2007).
[15] M. Kardar, G. Parisi, and Y.-C. Zhang, Phys. Rev. Lett. **56**, 889 (1986).
[16] Z.-W. Lai and S. Das Sarma, Phys. Rev. Lett. **66**, 2348 (1991).
[17] F. Ojeda, R. Cuerno, R. Salvarezza, and L. Vázquez, Phys. Rev. Lett. **84**, 3125 (2000).
[18] D. E. Wolf, Phys. Rev. Lett. **67**, 1783 (1991).
[19] H. Kallabis, J. Phys. A: Math. Gen. **31**, L581 (1998).
[20] H. Kallabis, Ph.D. thesis, Universität Duisburg, 1997.
[21] E. Vivo, M. Nicoli, M. Engler, T. Michely, L. Vázquez, and R. Cuerno, Phys. Rev. B **86**, 245427 (2012).

[22] C. Schelling, G. Springholz, and F. Schäffler, Phys. Rev. Lett. **83**, 995 (1999).
[23] M. Sato and M. Uwaha, Phys. Rev. E **60**, 7120 (1999).
[24] A. D. Verga, Phys. Rev. B **80**, 174115 (2009); arXiv:1207.4354.
[25] A. Ballestad, B. J. Ruck, M. Adamcyk, T. Pinnington, and T. Tiedje, Phys. Rev. Lett. **86**, 2377 (2001).
[26] A. Ballestad, B. J. Ruck, J. H. Schmid, M. Adamcyk, E. Nodwell, C. Nicoll, and T. Tiedje, Phys. Rev. B **65**, 205302 (2002).
[27] J. A. Sánchez-García, R. Gago, R. Caillard, A. Redondo-Cubero, J. A. Martin-Gago, F. J. Palomares, M. Fernández, and L. Vázquez, J. Phys.: Condens. Matter **21**, 224009 (2009).
[28] S. Macko, F. Frost, M. Engler, D. Hirsch, T. Höche, J. Grenzer, and T. Michely, New J. Phys. **13**, 073017 (2011).
[29] R. Cuerno, M. Castro, J. Muñoz-García, R. Gago, and L. Vázquez, Nucl. Instrum. Methods Phys. Res., Sect. B **269**, 894 (2011).
[30] E. Vivo, M. Nicoli, and R. Cuerno, Phys. Rev. E **86**, 051611 (2012).
[31] A. Keller, R. Cuerno, S. Facsko, and W. Möller, Phys. Rev. B **79**, 115437 (2009).
[32] A. Hansen, J. Schmittbuhl, and G. G. Batrouni, Phys. Rev. E **63**, 062102 (2001).
[33] B. Schmittmann, G. Pruessner, and H.-K. Janssen, Phys. Rev. E **73**, 051603 (2006).
[34] M. Henkel, H. Hinrichsen, and S. Lübeck, *Non-equilibrium Phase Transitions: Absorbing Phase Transitions* (Springer, Dordrecht, 2008), Vol. I.
[35] L. Ponson, D. Bonamy, and E. Bouchaud, Phys. Rev. Lett. **96**, 035506 (2006).
[36] E. Bouchbinder, I. Procaccia, and S. Sela, Phys. Rev. Lett. **95**, 255503 (2005).
[37] E. Bouchbinder, I. Procaccia, and S. Sela, J. Stat. Phys. **125**, 1025 (2006).
[38] T. Hwa and M. Kardar, Phys. Rev. Lett. **62**, 1813 (1989).
[39] T. Hwa and M. Kardar, Phys. Rev. A **45**, 7002 (1992).
[40] R. Cuerno and L. Vázquez, in *Advances in Statistical and Condensed Matter Physics*, edited by E. Korutcheva and R. Cuerno (Nova Science, New York, 2004).
[41] R. Cuerno, M. Castro, J. Muñoz-García, R. Gago, and L. Vázquez, Eur. Phys. J. Spec. Top. **146**, 427 (2007).
[42] U. C. Täuber and E. Frey, Europhys. Lett. **59**, 655 (2002).
[43] W. D. McComb, *The Physics of Fluid Turbulence* (Oxford University Press, New York, 1991).
[44] G. F. Mazenko, *Nonequilibrium Statistical Mechanics* (Wiley-VCH, Weinheim, 2006).
[45] C. A. Haselwandter and D. D. Vvedensky, Phys. Rev. Lett. **98**, 046102 (2007).
[46] M. Nicoli, R. Cuerno, and M. Castro, Phys. Rev. Lett. **102**, 256102 (2009).
[47] M. Nicoli, R. Cuerno, and M. Castro, J. Stat. Mech.: Theory Exp. (2011) P10030.
[48] A. Keller, M. Nicoli, S. Facsko, and R. Cuerno, Phys. Rev. E **84**, 015202(R) (2011).
[49] A. Keller, M. Nicoli, S. Facsko, and R. Cuerno, Phys. Rev. E **85**, 029905(E) (2012).
[50] H. K. Janssen, Phys. Rev. Lett. **78**, 1082 (1997).
[51] M. Nicoli, M. Castro, and R. Cuerno, Phys. Rev. E **78**, 021601 (2008).
[52] The same numerical simulation scheme has also allowed us to also check for the aKPZ equation (not shown), the change of universality class as a function of the relative signs of the nonlinearities when both are nonzero.
[53] A. A. Golovin and S. H. Davis, Physica D **116**, 363 (1998).
[54] S. Toh, H. Iwasaki, and T. Kawahara, Phys. Rev. A **40**, 5472 (1989).
[55] E. A. Kuznetsov, A. M. Rubenchik, and V. E. Zakharov, Phys. Rep. **142**, 103 (1986).
[56] E. A. Demekhin, E. N. Kalaidin, S. Kalliadasis, and S. Y. Vlaskin, Phys. Rev. E **82**, 036322 (2010).
[57] T. Hwa, Phys. Rev. Lett. **69**, 1552 (1992).
[58] A. J. Bray, A. Cavagna, and R. D. M. Travasso, Phys. Rev. E **64**, 012102 (2001).
[59] M. Rost and J. Krug, Phys. Rev. Lett. **75**, 3894 (1995).
[60] A. Karma and C. Misbah, Phys. Rev. Lett. **71**, 3810 (1993).
[61] M. Nicoli, E. Vivo, and R. Cuerno, Phys. Rev. E **82**, 045202(R) (2010).
[62] R. Cuerno and A.-L. Barabási, Phys. Rev. Lett. **74**, 4746 (1995).